An Accurate Description of the Bergman Reaction Using Restricted and Unrestricted DFT: Stability Test, Spin Density, and On-Top Pair Density†

Jürgen Gräfenstein, Angelica M. Hjerpe, Elfi Kraka,* and Dieter Cremer

Department of Theoretical Chemistry, Göteborg University, Reutersgatan 2, S-41320 Göteborg, Sweden

Received: September 2, 1999; In Final Form: November 29, 1999

DFT calculations provide a reliable description of the Bergman reaction of (Z)-hex-3-ene-1,5-diyne **1** provided the following are considered. (a) Restricted DFT (RDFT) calculations along the reaction path have to be replaced by unrestricted DFT (UDFT) calculations at those locations where the former description becomes unstable. This is the case in the region of the *p*-didehydrobenzene biradical **2**, which possesses significant multireference character. (b) LSD and pure GGA functionals are more stable than hybrid functionals, which can be directly related to the composition of these functionals. With increasing instability, RDFT calculations lead to increasing errors in the S−T splitting and the geometry of **2** as well as in the energetics of the Bergman reaction. (c) LSD and GGA functionals underestimate the energy barrier of the Bergman reaction of **1**. This becomes obvious when the correct experimental barrier is considered, which was not done in previous DFT investigations. (d) The best description of the Bergman reaction is provided by a mixed RDFT/UDFT description using the B3LYP functional (average error of 2.7 kcal/mol). Although the B3LYP functional is rather unstable, its semiempirical calibration helps to compensate for the typical underestimation of barriers by GGA functionals, which demonstrates that the performance of a hybrid functional does not necessarily have to do with its stability. (e) Application of the sum formula to the UB3LYP energy of biradical **2** improves the description of the Bergman reaction so that the most reliable data are obtained at RB3LYP-UB3LYP(sum)/6-311+G-(3df,3pd). Activation enthalpies at 470 K for forward and backward reaction are 29.9 and 21.4 kcal/mol, respectively (exptl values, 28.23 ± 0.5 and 19.75 ± 0.7 kcal/mol), while the calculated reaction enthalpy at 298 K is 8.5 kcal/mol (exptl value, 8.5 ± 1.0 kcal/mol) in reasonable agreement with experiment. The calculated S−T splitting is 2.6 kcal/mol (after correction, 4.9 kcal/mol; exptl value, 3.8 ± 0.5 kcal/mol at 298 K). It is shown that the UDFT description covers static correlation effects needed for the correct treatment of **2S**. Total and on-top pair density reflect this, while Kohn−Sham orbitals and spin density have to be considered as physically not meaningful intermediates in line with the interpretation given by Perdew, Savin, and Burke (*Phys. Rev. A* **1995**, *51*, 4531).

1. Introduction

Since the discovery of the enediyne antibiotics such as calicheamicin in the mid 1980's,[1] research on these compounds has led to a rapid increase in the understanding of the chemistry and biological activity of these compounds.[2,3] On the basis of this knowledge, much effort is channeled into the development of antitumor agents based on naturally occurring enediyne antibiotics. Calicheamicin, esperamicin, dynemicin, and other enediyne antibiotics are able to attack and destroy the DNA of tumor cells. The key role in this attack plays a Bergman cyclization[4] of the enediyne kernel to *p*-didehydroarene biradicals and subsequent H abstraction from DNA by the biradical. Consequently, much of the experimental and theoretical work has focused on the Bergman reaction. Kinetic experiments by Roth, Hopf, and Horn[5] described the energetics of the Bergman cyclization of the parent enediyne, (*Z*)-hex-3-ene-1,5-diyne **1** (see Figure 1). The *p*-didehydrobenzene biradical **2** was isolated for the first time at low temperature in the matrix and characterized with infrared measurements in combination with quantum chemical calculations by Sander and co-workers.[6] Other work studied the reactivity of enediynes in dependence on their structure.[7] For example, it was shown that incorporation of the enediyne unit into a nine- or ten-membered ring as in the case of the naturally occurring enediynes lowers the barrier to Bergman cyclization so that a potential drug can become active at body temperature.[7] It was also investigated whether a modification of the enediyne by incorporation of a N atom can improve its biological activity.[8]

A large impact on the progress in enediyne chemistry was provided by quantum chemical calculations. First calculations on the Bergman reaction of the parent compound used ab initio theory ranging from MRDCI, CCSD(T), and BD(T) to CASSCF or CASSCF−PT2 calculations.[9] The most reliable results on the energetics of the Bergman reaction were obtained at the CCSD(T)/VDZP level by Kraka and Cremer,[10] although calculations with extended basis sets showed that CCSD(T) underestimates somewhat the stability of the biradical **2**,[9f] which possesses a (low-spin) open-shell singlet (S) ground state **2S** and, therefore, is more difficult to calculate than the first excited state, namely the triplet (T) state **2T**, which is 3.8 kcal/mol higher in energy than the S state according to experiment.[11] CASSCF and CASSCF-PT2 calculations turned out to overestimate the stability of **2S**[9f] where it seems to be a general problem to bring static and dynamic electron correlation effects into the right balance for molecules with different π-systems

* Corresponding author. E-mail: Cremer@theoc.gu.se.

† Presented in part at the WATOC 99 conference, London, 1999.

10.1021/jp993122q CCC: $19.00
Published on Web 02/05/2000

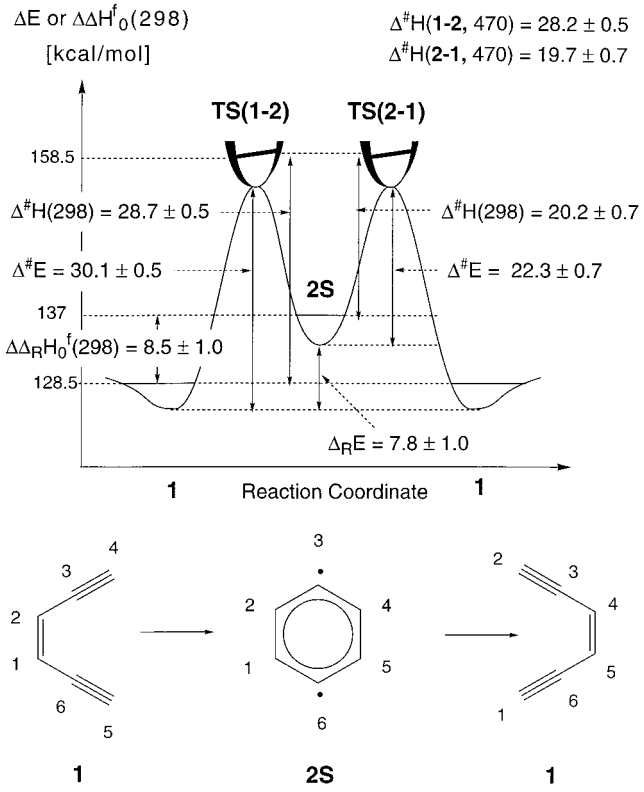

Figure 1. Energy profile of the Bergman reaction of (*Z*)-hex-3-ene-1,5-diyne **1** as determined by experiment.[5] The experimental reaction enthalpy $\Delta\Delta H_0^f(298)$, the activation enthalpies for forward and backward reaction, $\Delta H^{\ddagger}$(**1**−**2**,470) and $\Delta H^{\ddagger}$(**2**−**1**,470), respectively, are converted to both enthalpy differences at 298 K and energy differences at 0 K ($\Delta_R E$, $\Delta E^{\ddagger}$(**1**−**2**), $\Delta E^{\ddagger}$(**2**−**1**)) using vibrational corrections calculated at the B3LYP/6-311+G(3df,3pd) level of theory. The numbering of C atoms for **1** and **2** is done in a consistent way, thus refraining from the IUPAC numbering for **1** and **2**.

(**1**, 10 π electrons; **2**, 6 π electrons, 2 single electrons in in-plane orbitals).

Theoretical research on enediyne antibiotics does not just focus on the parent system but also on more realistic enediyne units such as cyclononenediynes and cyclodecenediynes as they occur in the natural products.[7,12,13] Actually, one wants to investigate besides the enediyne warhead also the trigger device and the docking system[3] of the naturally occurring enediynes. Clearly, this is no longer possible using CCSD(T) or other advanced ab initio methods because of the cost factor implied. This was the major motivation for testing the performance of density functional theory (DFT) methods for the description of the Bergman reaction of the parent system and some modified enediynes.[6,9g,9h,12,13] Functionals based on the generalized gradient approximation (GGA) or, in addition, on empirically adjusted hybrid functionals perform surprisingly well when describing the Bergman cyclization reaction and, therefore, much work was done to find the most reliable functional. A recent study by Chen and co-workers[13] tested four different functionals at restricted DFT (RDFT) with different basis sets and compared their performance with more advanced methods such as CCSD(T) and CASSCF-PT2. These authors came to different conclusions as the authors of earlier DFT work performed at the unrestricted DFT (UDFT) level of theory,[6,9g,9h] particularly to calculate the properties (geometry and vibrational frequencies) of the biradical **2S** appropriately.[6] Hence, there are presently two approaches in the literature to describe enediynes and their cyclization reaction where one is based on RDFT[12,13] and one on UDFT[6,9g,9h] and each of them suggests different functionals for the optimal description of enediynes by DFT.

We will show in this work that the use of RDFT for the description of the Bergman reaction is misleading because restricted theory becomes externally unstable and a more stable UDFT solution exists. Accordingly, the calculated R energy and geometry of biradical **2S** are unreasonable (not discussed in previous work) and do not provide reliable information on the performance of the functionals used. Apart from this, the basic question has to be considered as to how a multireference problem such as biradical **2S** can be reasonably described with single-determinant Kohn−Sham (KS) DFT.[14] Clearly, all wave function studies of **2S** indicate the need of the coverage of both dynamic and static electron correlation effects, which cannot be provided by RDFT. We will demonstrate that UDFT covers indirectly static correlation effects (besides the dynamic correlation effects covered by the exchange-correlation functional XC) and will discuss the performance of UDFT with the help of spin density and on-top pair density. An important conclusion of this work is that future work on enediynes can be performed with DFT provided the stability of all RDFT calculations is tested and the advantages of UDFT as described in this work are exploited. Suggestions for the use of functionals and basis sets with the best performance will be made.

2. Computational Procedures

Throughout this work, DFT[14] was employed using seven different functionals and four different basis sets. The functionals were chosen to represent the local spin density (LSD) approach, the generalized gradient approximation (GGA), or a hybrid functional method.[15] For LSD, the SVWN functional was chosen, which combines the Slater exchange[16] functional with the Vosko−Wilk−Nusair correlation functional.[17] SVWN is based on the homogeneous electron gas and covers local exchange and local correlation effects. The three GGA functionals employed in this work are BP86,[18,19] BPW91,[18,20] and BLYP.[18,21] All three use the Becke88 exchange functional[18] based on Slater exchange and corrections involving the gradient of the density, thus adding nonlocal exchange effects.[22] P86 is Perdew's gradient-corrected correlation functional,[19] PW91 is the Perdew−Wang (1991) gradient-corrected correlation functional,[20] and LYP is the correlation functional of Lee, Yang, and Parr,[21] which is a modification of the Colle and Salvetti correlation energy formula.[23] The three hybrid functionals used are Becke's three-parameter functionals B3LYP and B3PW91[24] and the one-parameter functional mPW1PW91 of Barone and Adamo[25] based on the modified Perdew−Wang exchange functional mPW91 and the Perdew−Wang (1991) correlation functional. We have chosen mPW1PW91 to represent a promising member of the new class of one-parameter hybrid functionals, which have been further optimized to extend the applicability of DFT.[26] For B3LYP and B3PW91, the same fitting parameters ($a_0 = 0.80$, $a_X = 0.72$, and $a_C = 0.81$ in the notation of ref 24a) are taken. The single parameter of mPW1PW91, which mixes Hartree−Fock (HF) and DFT exchange, is 0.25 as determined by lowest order Görling−Levy perturbation theory.[25]

Explorative calculations were made with a variety of VDZ and VTZ basis sets. Results obtained with the 6-31G(d,p)[27] basis and Dunning's cc-pVDZ[28] were similar. Since Pople's 6-31G(d,p) basis is used more frequently than the corresponding Dunning basis, we decided to use the former. On the other hand, we decided to use Dunning's cc-pVTZ basis set,[29] which is composed of a (10s5p2d1f/5s2p1d)[4s3p2d1f/3s2p1d] contrac-

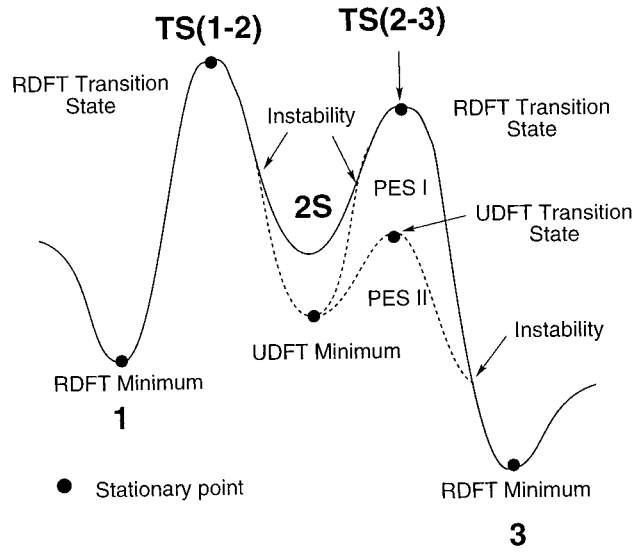

Figure 2. Schematic drawing of the energy profile of the Bergman cyclization of an unsymmetrical enediyne. The RDFT potential energy surface (PES) is given by a solid line. Regions of instability of the RDFT solution are indicated by dashed lines. Two situations are considered for the reaction **2S** → **3**. (a) The RDFT solution for **TS-(2−3)** is stable. The region of instability is constrained to the vicinity of **2S**. (b) The RDFT solution for **TS(2−3)** is unstable.

tion. As an even larger basis, Pople's 6-311+G(3df,3pd) basis[30] was employed to get the best results presented in this work. Hence, we report here the energetics of the Bergman reaction for 15 different functional/basis set combinations applying the following procedure. (1) For each functional/basis set employed, the equilibrium geometry of enediyne **1**, singlet biradical **2S**, and transition state **TS(1−2)** (see Figure 1) were calculated at RDFT. Vibrational frequencies were determined to characterize the stationary points found as minimum or first-order saddle point. Then, the internal and external stability of the R solution of **1**, **2S**, and **TS(1−2)** were calculated with the help of the Hermitian stability matrices **A** and **B**.[31] All RDFT calculations turned out to be internally stable, however, for biradical **2S** the external stability matrix **B** possessed one negative eigenvalue λ, indicating a breaking of the constraint $\psi_\alpha = \psi_\beta$. The more negative λ is, the larger is the observed instability.[31,32] The corresponding eigenvector leads outside the restricted subspace, thus yielding an UDFT energy lower than the RDFT energy. Reoptimization of the geometry at UDFT leads to an energy lowering ΔE(U−R), which can be considered as a second parameter describing the instability of the RDFT solution.

Considering the energy profile of the Bergman reaction in the general case of an asymmetrically substituted enediyne, there are several locations where external stability of the RDFT description can be expected (see Figure 2). Clearly, the reactant **1** represents a typical closed-shell system and, therefore, the RDFT solution should be internally and externally always stable. However, external instability could occur in the TS regions or in the vicinity of the biradical **2S** (see Figure 2). For enediynes with heteroatoms, we observed both cases,[33] while for the parent enediyne system investigated in this work just the latter case was found. Hence, the UDFT PES, which collapses in several regions with the RDFT PES, was taken to describe the energetics of the Bergman reaction.

For the biradical **2**, the lowest T state was calculated at UDFT employing the same functional/basis set combinations used for the calculation of the corresponding S state. Besides the parameters λ and ΔE(U−R), the calculated S−T splitting was used to evaluate R and U descriptions of the S state.

Three different ways were followed to assess the reliability of the UDFT description of the S state of biradical **2**.

(1) The expectation value $\langle \hat{S}^2 \rangle$ was calculated with the help of Kohn−Sham (KS) orbitals and used to correct the UDFT energy for **2S** according to the sum formula[34]

$$E(\mathrm{UDFT},\mathbf{2S}) = xE(\mathbf{2S}) + (1-x)E(\mathbf{2T}) \tag{1a}$$

$$E(\mathbf{2S}) = \frac{1}{x}E(\mathrm{UDFT},\mathbf{2S}) - \frac{(1-x)}{x}E(\mathbf{2T}) \tag{1b}$$

where x is determined from eq 2

$$\langle \hat{S}^2 \rangle_{\mathrm{UDFT},\mathbf{2S}} = x\langle \hat{S}^2 \rangle_{\mathbf{2S}} + (1-x)\langle \hat{S}^2 \rangle_{\mathbf{2T}} \tag{2a}$$

$$x = \frac{\langle \hat{S}^2 \rangle_{\mathrm{UDFT},\mathbf{2S}} - \langle \hat{S}^2 \rangle_{\mathbf{2T}}}{\langle \hat{S}^2 \rangle_{\mathbf{2S}} - \langle \hat{S}^2 \rangle_{\mathbf{2T}}} \tag{2b}$$

The sum formula is based on two assumptions, namely, (a) that the expectation value $\langle \hat{S}^2 \rangle$ can be calculated from KS orbitals and (b) that the predominant contamination of the S state results from the T. Both assumptions have to be discussed in this work.

(2) The spin density (spin magnetization density) distribution $m_s(\mathbf{r}) = \rho_\alpha(\mathbf{r}) - \rho_\beta(\mathbf{r})$ was calculated for the S state at UDFT and compared with that of the T state to obtain $\langle \hat{S}^2 \rangle$ in an alternative way. Again, the value of $\langle \hat{S}^2 \rangle$ was used to correct the S energy with the help of the sum formula 1.

(3) The on-top pair density $P(\mathbf{r},\mathbf{r})$[35,36] (see section 4) was calculated to describe S and T state of the biradical **2**.

The performance of the various functionals and basis sets employed was tested by comparison with the experimental energy data shown in Figure 1. Since all three energy parameters are important for the characterization of the Bergman reaction (e.g., the barrier via **TS(2−1)** determines the kinetic stability and, by this, the lifetime of the biradical **2S**), the performance of the various functionals and basis sets was determined by calculating absolute mean deviations μ as well as the corresponding standard deviations σ with regard to three rather than two energy parameters.

The numbering of atoms in **1**, **TS(1−2)**, and **2** was done consistently as indicated in Figure 1. Calculations were carried out with the programs COLOGNE 99[37] and Gaussian 98[38] where the former provides possibilities of analyzing $m_s(\mathbf{r})$ and $P(\mathbf{r},\mathbf{r})$.

3. Stability of the Restricted DFT Description of the Bergman Reaction

When comparing calculated energies with the experimental enthalpy data of Roth and co-workers,[5] one has to consider that the experimental reaction enthalpy $\Delta\Delta H_0^f$ was determined at 298 K ($\Delta\Delta H_0^f(298) = 8.5 \pm 1.0$ kcal/mol), while the activation enthalpies $\Delta H^\ddagger(\mathbf{1}-\mathbf{2})$ and $\Delta H^\ddagger(\mathbf{2}-\mathbf{1})$ for forward and backward reaction (Figure 1) were measured at 470 K ($\Delta H^\ddagger(\mathbf{1}-\mathbf{2},470) = 28.2 \pm 0.5$ and $\Delta H^\ddagger(\mathbf{2}-\mathbf{1},470) = 19.7 \pm 0.7$ kcal/mol). Since the vibrational frequencies of **1** and **TS(1−2)** are experimentally not known, the most accurate DFT description (see section 3) was applied to calculate zero-point energies (ZPE) and temperature corrections for the experimental enthalpies at 298 and 470 K. In this way, one obtains the activation enthalpies at 298 K $\Delta H^\ddagger(\mathbf{1}-\mathbf{2},298) = 28.7 \pm 0.5$ and $\Delta H^\ddagger(\mathbf{2}-\mathbf{1},298) = 20.2 \pm 0.7$ kcal/mol and the energy differences at 0 K (without ZPE corrections, $\Delta_R E = 7.8 \pm 1.0$, $\Delta E^\ddagger(\mathbf{1}-\mathbf{2}) = 30.1 \pm 0.5$, and $\Delta E^\ddagger(\mathbf{2}-\mathbf{1}) = 22.3 \pm 0.7$ kcal/mol) shown in Figure 1. This procedure is slightly flawed by the fact that at higher temperatures the harmonic description of vibrational modes is no longer

TABLE 1: RDFT and UDFT Descriptions of *para*-Didehydrobenzene Biradical 2S[a]

functional	basis set	λ	ΔE(U−R)	ΔR (RDFT)	ΔR (UDFT)	ratio η (RDFT)	ratio η (UDFT)
SVWN	6-31G(d,p)	−0.0118	−1.3	0.118	0.083	1.088	1.061
SVWN	cc-pVTZ	−0.0084	−0.8	0.124	0.092	1.093	1.068
BP86	6-31G(d,p)	−0.0295	−5.9	0.125	0.063	1.092	1.046
BP86	cc-pVTZ	−0.0269	−5.2	0.132	0.069	1.098	1.050
BPW91	6-31G(d,p)	−0.0325	−7.0	0.126	0.059	1.093	1.060
BPW91	cc-pVTZ	−0.0299	−6.4	0.132	0.064	1.098	1.047
BLYP	6-31G(d,p)	−0.0303	−5.3	0.129	0.069	1.095	1.050
BLYP	cc-pVTZ	−0.0267	−4.4	0.136	0.075	1.101	1.055
B3PW91	6-31G(d,p)	−0.0716	−19.1	0.133	0.045	1.099	1.033
B3PW91	cc-pVTZ	-[b]	−17.9	0.138	0.048	1.103	1.035
B3LYP	6-31G(d,p)	−0.0696	−17.3	0.134	0.048	1.100	1.035
B3LYP	cc-pVTZ	−0.0643	−15.7	0.140	0.053	1.105	1.039
B3LYP	6-311+G(3df,3pd)	-[b]	−15.4	0.140	0.053	1.105	1.039
MPW1PW91	6-31G(d,p)	−0.0832	−23.1	0.132	0.042	1.098	1.031
MPW1PW91	cc-pVTZ	-[b]	−21.8	0.138	0.045	1.103	1.033

[a] Energy differences ΔE(U−R) in kcal/mol, bond length differences $\Delta R = R$(C1C2) − R(C2C3) in Å. The parameter λ is the lowest eigenvalue of the stability matrix. $\lambda < 0$ indicates instability with regard to an external perturbation of the RDFT solution. The ratio $\eta = R$(C1C2)/R(C2C3) is a parameter for bond equilibration in **2S**. [b] The stability test could not be carried out because of two degenerate λ values.

TABLE 2: Energetics of the Bergman Cyclization of Enediyne 1 Calculated at Various Levels of DFT[a]

functional	basis set	energy of **1**	$\Delta E^{\ddagger}$(**1**−**2**)	$\Delta_R E$	$\Delta E^{\ddagger}$(**2**−**1**)	μ	σ
SVWN	6-31G(d,p)	−229.51163	17.7	−4.6	22.3	8.3	7.1
SVWN	cc-pVTZ	−229.60115	19.2	0.6	18.6	7.3	3.6
BP86	6-31G(d,p)	−230.87735	22.4	0.6	21.8	5.1	4.0
BP86	cc-pVTZ	−230.95911	24.6	6.0	18.5	3.7	1.8
BPW91	6-31G(d,p)	−230.85529	23.3	0.2	23.1	5.1	3.7
BPW91	cc-pVTZ	−230.93501	25.4	5.4	20.0	3.1	1.4
BLYP	6-31G(d,p)	−230.79499	25.4	6.8	18.6	3.1	1.9
BLYP	cc-pVTZ	−230.88542	28.6	13.6	15.1	4.8	2.9
B3PW91	6-31G(d,p)	−230.78776	28.9	−2.8	31.8	7.1	5.1
B3PW91	cc-pVTZ	−230.86567	31.2	2.7	28.5	4.1	2.7
B3LYP	6-31G(d,p)	−230.88718	31.2	3.3	27.9	3.7	2.3
B3LYP	cc-pVTZ	−230.97270	34.4	10.1	24.3	2.9	1.3
B3LYP	6-311+G(3df,3pd)	−230.96868	34.1	10.1	24.0	2.7	1.2
MPW1PW91	6-31G(d,p)	−230.81666	29.6	−5.6	35.2	8.9	7.3
MPW1PW91	cc-pVTZ	−230.89424	31.8	−0.1	31.9	6.4	4.2
experimental			30.1 ± 0.5	7.8 ± 1.0	22.3 ± 0.7		

[a] Absolute energies in hartree, relative energies in kcal/mol. $\Delta E^{\ddagger}$(**1**−**2**), $\Delta_R E$, and $\Delta E^{\ddagger}$(**2**−**1**) denote the barrier for the forward reaction, the reaction energy, and the barrier for the backward reaction, respectively. The mean absolute deviation μ and the standard deviation σ are calculated with regard to the experimental values taken from ref 5 and corrected to energies at 0 K (see Figure 1 and text).

accurate. However, the difference in the activation enthalpy at 298 and 470 K is nonnegligible (0.5 kcal/mol) and larger than possible errors because of anharmonicity effects not considered for temperature corrections up to 470 K. We note that in previous DFT investigations these differences were not considered and that previous conclusions on the performance of DFT in the case of the Bergman reaction were slightly flawed by this.[12,13] In this work, we reference all calculated energies to the experimentally based reaction energy and energy barriers at 0 K shown in Figure 1 because we will discuss preferentially electronic effects influencing the stability of **1**, **TS(1−2)**, **2S**, and **2T**.

In Table 1, the RDFT description of biradical **2S** is compared with the corresponding UDFT description. For all functionals and basis sets considered, the R solution is externally unstable and a more stable U solution exists. This important aspect has not been considered in some of the previous DFT investigations of the Bergman reaction[12,13] although it changes the calculated energetics considerably as can be seen from the energy difference ΔE(U−R) = E(**2S**,UDFT) − E(**2S**,RDFT) (Table 1). Tables 2 and 3 list the energy data of the Bergman reaction (energy barrier $\Delta E^{\ddagger}$(**1**−**2**), reaction energy $\Delta_R E$, and reaction barrier $\Delta E^{\ddagger}$(**2**−**1**) as well as calculated S−T splittings. The RDFT splittings have the wrong sign (in most cases) and differ from the experimental value (3.8 ± 0.5 kcal/mol at 298 K[11]) by up to 23 kcal/mol. The energetics of the Bergman reaction is also poorly described at RDFT for most functionals. It was these observations that led to misleading claims that hybrid functionals are not suitable for describing the Bergman reaction.[12,13] We note that these claims were made without testing the stability of the R solutions.

Stability Tests. The RDFT description for **1** and **TS(1−2)** is stable at all DFT levels considered although the lowest eigenvalue λ of the external stability matrix was just 0.0060 at B3LYP/6-31G(d,p) (at SVWN/6-31G(d,p), 0.0739). The calculated eigenvalues of the stability matrix indicate that the instability of the R solution for **2S** increases in the order SVWN < BLYP, BP86 < BPW91 < B3LYP < B3PW91 < mPW1PW91 and VTZP basis set < VDZP basis set.

Absolute differences ΔE(U−R) increase parallel to this trend from 1 to 23 kcal/mol (Table 1). There is a quadratic relationship between ΔE(U−R) and the eigenvalue λ, which can be used to predict changes in energy from calculated λ values. A LSD functional such as SVWN is more stable than a GGA functional such as BLYP, which in turn is more stable than a hybrid functional such as B3LYP. This is parallel to what Bauernschmitt and Ahlrichs[31] reported and what can be expected from the construction of the functionals used. Normally, an R solution is the more stable the more correlation effects are covered by the method in question. Clearly, LSD, which is based on the electron correlation of the homogeneous electron gas and is

TABLE 3: Singlet−Triplet Splitting of *p*-Didehydrobenzene 2 Calculated at Various Levels of DFT[a]

functional	basis set	energy of **2T**	S−T(RDFT) splitting	S−T(UDFT) splitting	$\langle\hat{S}^2\rangle_{KS}$	correct. eq 1	$\Delta E^{\#}$(**1**−**2**) correct.	$\Delta_R E$ correct.	S−T(correct.) splitting	μ	σ
SVWN	6-31G(d,p)	−229.50932	4.7	6.1	0.57	2.4	15.3	−7.1	8.5	8.7	7.4
SVWN	cc-pVTZ	−229.58957	5.8	6.6	0.49	2.2	17.1	−1.5	8.8	7.8	4.2
BP86	6-31G(d,p)	−230.87036	−2.1	3.8	0.84	2.7	19.7	−2.1	6.5	5.9	5.0
BP86	cc-pVTZ	−230.94311	−1.2	4.0	0.81	2.7	21.9	3.3	6.7	4.9	2.3
BPW91	6-31G(d,p)	−230.84949	−3.6	3.5	0.87	2.6	20.7	−2.5	6.1	5.8	4.8
BPW91	cc-pVTZ	−230.92059	−2.8	3.6	0.85	2.7	22.8	2.8	6.3	4.4	2.3
BLYP	6-31G(d,p)	−230.77758	−1.2	4.1	0.80	2.7	22.6	4.1	6.9	4.6	1.9
BLYP	cc-pVTZ	−230.85665	0.1	4.5	0.77	2.8	25.8	10.8	7.3	4.6	1.9
B3PW91	6-31G(d,p)	−230.78853	−16.8	2.3	0.97	2.2	26.7	−5.0	4.5	6.7	5.4
B3PW91	cc-pVTZ	−230.85759	−15.6	2.4	0.96	2.2	29.0	0.5	4.6	3.9	3.3
B3LYP	6-31G(d,p)	−230.87800	−14.8	2.5	0.95	2.2	28.9	1.1	4.7	3.7	2.9
B3LYP	cc-pVTZ	−230.95254	−13.1	2.6	0.94	2.3	32.1	7.8	4.9	1.4	0.9
B3LYP	6-311+G(3df,3pd)	−230.94840	−12.8	2.6	0.94	2.3	31.8	7.8	4.9	1.2	0.8
MPW1PW91	6-31G(d,p)	−230.82207	−20.9	2.2	0.99	2.1	27.5	−7.7	4.3	7.9	7.3
MPW1PW91	cc-pVTZ	−230.89086	−19.6	2.2	0.98	2.1	29.7	−2.1	4.3	5.2	5.3
exptl[11]			3.5 ± 0.5[b]	3.5 ± 0.5[b]	0	0	30.1 ± 0.5	7.8 ± 1.0	3.5 ± 0.5[b]		

[a] Absolute energies in hartree, relative energies in kcal/mol. The expectation value $\langle\hat{S}^2\rangle_{KS}$ was calculated with the KS orbitals. Correct. denotes the energy correction fot the S−T splitting calculated at the UDFT level when the sum formula (eq 1) is applied; that is, it gives the energy in kcal/mol, by which the energy of **2S** is lowered. This correction leads also to changes in the energetics of the Bergman reaction ($\Delta E^{\ddagger}$(**1**−**2**), and $\Delta_R E$ while $\Delta E^{\ddagger}$(**2**−**1**) does not change) and to revised mean absolute deviation μ and standard deviation σ, which are given in the last two columns. [b] Experimental value corrected to 0 K.

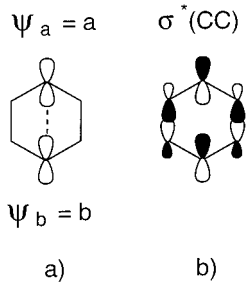

Figure 3. Spin-coupling mechanisms possibly active in biradical **2S**. (a) Through-space interactions between single electron orbitals $\psi_a = a$ and $\psi_b = b$ as indicated by the dashed line. (b) Through-bond interactions involving the σ*(CC) orbitals of the HCCH fragments.

known to exaggerate correlation energies of inhomogeneous systems, is more stable than GGA functionals.

Mixing of HF exchange leads to larger instability of the R description of **2S** because HF is always less stable than DFT in practical applications.[31,32] Since the mPW1PW91 functional[25] contains more HF exchange than the B3LYP and B3PW91 functionals, RDFT results of the former are less stable than those of the latter. The larger stability of B3LYP relative to B3PW91 seems to be a consequence of the larger stability of results obtained with the LYP correlation functional than those obtained with the PW91 functional.

It is well-known that, at the HF level of theory an extension of the basis set increases the stability of the R solution. This holds also for DFT as is reflected by the calculated stability parameters λ and the differences ΔE(U−R), although the changes are relatively small. For example, the differences ΔE(U−R) are reduced by just 0.5 to 1.5 kcal/mol (see Table 1).

RDFT and UDFT geometries of **2S** differ in a typical way. The R description of biradical **2S** requires a strong coupling between the two single electrons, which can proceed by two different mechanisms (see Figure 3): (1) through-space mechanism depending on the distance between C3 and C6 (Figure 3a); (2) through-bond mechanism depending on orbital interactions as indicated in Figure 3b.

The first mechanism requires a sufficiently short distance (2.0−2.4 Å) between C3 and C6 to guarantee significant overlap between local orbitals $\psi_a = a$ and $\psi_b = b$. Tables 4 and 5 list the geometries calculated in this work, which reveal that calculated C3C6 distances of **2S** are too large for important through-space interactions. The through-bond mechanism is more effective, the larger the overlap is (Figure 3) and the smaller the orbital energy difference between orbitals *a* and *b* and low-lying antibonding orbitals is. Hoffmann and coworkers[39] showed that the σ*(CC) orbitals (Figure 3b) are most effective in this connection.

The RDFT description enforces strong through-bond coupling between the single electrons and, consequently, the four bonds of the type C2C3 become relatively short (increase of in-plane π-type overlap) while those of the type C1C2 become relatively long (occupation of a CC antibonding orbital). This is documented by the geometrical parameter $\Delta R = R$(C1C2) − R(C2C3) and the bond equilibration ratio $\eta = R$(C1C2)/R(C2C3) (see Table 1). The RDFT parameters ΔR and η are relatively large compared to the corresponding UDFT parameters. Hence, the RDFT geometry of **2S** describes the biradical as an unrealistic assembly of two allyl units interacting via two relatively long bonds C1C2 and C4C5. This was overlooked in previous RDFT investigations of **2S**.[12,13]

Use of the UDFT description of **2S** leads to the following improvements. (1) A reasonable geometry results, which is indirectly confirmed by comparison of the associated vibrational frequencies with the available experimental data.[6] (2) The calculated S−T splittings (Table 3) agree better with the experimental value of 3.5 kcal/mol.[11] (3) The energetics of the Bergman reaction is in better agreement with experimental data[5] (Figure 1, Table 2).

While there is no question that one has to use the broken-symmetry solution, it is not clear apriori which of the functionals leads to the best description. In the literature, the suggestion was that a pure functional such as BLYP should perform better than a hybrid functional such as B3LYP because the latter should suffer from similar deficiencies as HF does in the case of a multireference problem.[8b,12,13] One could see the results on the stability of the various functionals (Table 1) as a confirmation of that view insofar as RB3LYP leads to a more unstable solution than RBLYP. However, we note that the stability of the R solution obtained with a given functional does not necessarily parallel the performance of the U description obtained with the same functional, although an increase of

TABLE 4: Geometrical Parameters of Enediyne 1 and Transition State TS(1−2)[a]

functional	basis set	*R*(C1C2)	*R*(C2C3)	*R*(C3C4)	*R*(C4C5)	α(C1C2C3)	α(C2C3C4)
			Enediyne **1**				
SVWN	6-31G(d,p)	1.357	1.399	1.219	4.404	124.6	182.2
SVWN	cc-pVTZ	1.349	1.395	1.209	4.350	124.5	181.6
BP86	6-31G(d,p)	1.369	1.415	1.225	4.526	125.4	182.8
BP86	cc-pVTZ	1.362	1.411	1.216	4.485	125.5	182.2
BPW91	6-31G(d,p)	1.368	1.415	1.223	4.538	125.6	182.8
BPW91	cc-pVTZ	1.360	1.410	1.214	4.502	125.7	182.3
BLYP	6-31G(d,p)	1.370	1.418	1.223	4.547	125.7	182.8
BLYP	cc-pVTZ	1.362	1.414	1.214	4.522	125.9	182.4
B3PW91	6-31G(d,p)	1.353	1.415	1.212	4.462	125.3	182.1
B3PW91	cc-pVTZ	1.346	1.411	1.204	4.436	125.4	181.9
B3LYP	6-31G(d,p)	1.355	1.417	1.211	4.478	125.3	182.4
B3LYP	cc-pVTZ	1.347	1.413	1.203	4.456	125.5	182.1
MPW1PW91	6-31G(d,p)	1.350	1.414	1.210	4.490	125.1	182.1
MPW1PW91	cc-pVTZ	1.344	1.410	1.202	4.417	125.2	181.9
			TS(1−2)				
SVWN	6-31G(d,p)	1.392	1.385	1.253	2.178	118.4	139.2
SVWN	cc-pVTZ	1.388	1.379	1.245	2.105	118.1	138.5
BP86	6-31G(d,p)	1.408	1.402	1.268	2.123	118.9	136.4
BP86	cc-pVTZ	1.405	1.393	1.262	2.062	118.5	136.0
BPW91	6-31G(d,p)	1.407	1.401	1.267	2.120	118.9	136.5
BPW91	cc-pVTZ	1.403	1.392	1.261	2.061	118.5	136.1
BLYP	6-31G(d,p)	1.413	1.403	1.273	2.073	119.0	135.0
BLYP	cc-pVTZ	1.410	1.393	1.267	2.008	118.6	134.5
B3PW91	6-31G(d,p)	1.400	1.385	1.260	1.929	118.3	133.6
B3PW91	cc-pVTZ	1.395	1.385	1.255	1.966	118.2	134.6
B3LYP	6-31G(d,p)	1.402	1.395	1.265	1.978	118.7	133.8
B3LYP	cc-pVTZ	1.400	1.385	1.260	1.925	118.3	133.5
MPW1PW91	6-31G(d,p)	1.395	1.392	1.259	1.996	118.5	134.6
MPW1PW91	cc-pVTZ	1.393	1.384	1.254	1.949	118.2	134.4

[a] Distances in Å; bond angles α in degree.

dynamic correlation effects will carry over to a certain degree to the UDFT level of theory. At the UDFT level, static correlation effects are also included (see section 4), which can be increased by the parametrization of the functional in the case of hybrid methods.[40] In view of these considerations, the performance parameters μ (absolute mean deviation) and σ (standard deviation) listed in Table 2 become understandable:

Both the most stable (SVWN) and the least stable functionals (mPW1PW91 and B3PW91) perform poorly, although some improvements are obtained when using the cc-pVTZ basis instead of the smaller 6-31G(d,p) basis. The GGA functionals perform reasonably with the larger basis set where a good agreement between theory and experiment is provided by BPW91/cc-pVTZ (μ = 3.1 kcal/mol; Table 2). The BLYP functional leads to the best values when using the 6-31G(d,p) basis (μ = 3.1 kcal/mol; Table 2), however performs worse with the cc-pVTZ basis (μ = 4.8 kcal/mol), which raises doubts with regard to claims on the superiority of the BLYP functional for describing the Bergman reaction.[8b,12] The best performance of DFT is obtained at the B3LYP/cc-pVTZ level of theory (μ = 2.9 kcal/mol). B3LYP performs better than any of the other functionals tested, which was the reason to further improve the basis set at this level of theory. At B3LYP/6-311+G(3df,3pd), the mean deviation is just 2.7 and the standard deviation just 1.2 kcal/mol. Clearly, this is a result of the calibration of the functional with the help of experimental data and the additional static correlation effects included at the UDFT level (see section 4).

Barriers calculated with SVWN or one of the GGA functionals are all too small by 3−13 kcal/mol. It is a well-known fact that reaction barriers tend to be underestimated by DFT, especially in the case of LSD and GGA functionals.[41] Also, calculated reaction energies are underestimated; however, there is no regularity in deviations from experimental energies so that an empirical correction of LSD and GGA energies is difficult. The B3LYP/6-311+G(3df,3pd) results (34.1, 10.1, 24.0 kcal/mol; Table 2) are too large by 4.0, 2.3, and 1.7 kcal/mol (Table 2), which suggests the possibility of further improving B3LYP energies (see below).

Apart from the SVWN result, all S−T splittings obtained at UDFT are reasonable, ranging from 2.2 to 4.5 kcal/mol thus bracketing the experimental value of 3.5 kcal/mol.[11] The GGA functionals perform better than the hybrid functionals, however differences are marginal. The B3LYP/6-311+G(3df,3pd) value (2.6 kcal/mol, Table 3) is 1.2 kcal/mol too small. Suggestions have been made to use $\langle \hat{S}^2 \rangle$ obtained from Kohn−Sham orbitals and to apply sum formula (1) to improve UDFT results for the S−T splitting.[34] According to Table 3, the application of eq 1 leads to an increase of S−T splittings by 2−3 kcal/mol and, by this, to values that are 2.3−4.7 and 0.5−1.1 kcal/mol too large in the case of the GGA and the hybrid functionals, respectively. The energetics of the Bergman reaction predicted with the help of sum formula (1) is equally or less accurate than at the UDFT level. Clearly, this indicates that sum formula (1) should be used in DFT either in a more educated way or not at all. The use of (1) will make sense if there is an equal mixing of S and T in the UHF description of a S biradical. Since B3LYP and other hybrid functionals include a significant part of HF exchange, one can argue that the application of the sum formula is justified in these cases, while in the case of pure density functionals it should be avoided since spin contamination plays a smaller role in DFT than in wave function theories such as HF.

For UB3LYP, use of the sum formula (1) leads to a stabilization of **2S** by 2.1−2.3 kcal/mol (Table 3), which means that the Bergman reaction becomes less endothermic (more exothermic). According to the Hammond postulate, a more exothermic reaction possesses a lower barrier and, therefore, it is reasonable to apply the sum formula correction also to the

TABLE 5: Geometrical Parameters of the S and T State of the *p*-Didehydrobenzene Biradical 2 as Calculated at RDFT and UDFT[a]

functional	basis set	*R*(C1C2)	*R*(C2C3)	*R*(C3C6)	α(C1C2C3)	α(C2C3C4)
			2S, RDFT			
SVWN	6-31G(d,p)	1.462	1.344	2.716	117.8	124.4
SVWN	cc-pVTZ	1.459	1.335	2.692	117.5	125.0
BP86	6-31G(d,p)	1.482	1.357	2.751	117.9	124.3
BP86	cc-pVTZ	1.480	1.348	2.726	117.5	125.0
BPW91	6-31G(d,p)	1.481	1.355	2.747	117.8	124.3
BPW91	cc-pVTZ	1.479	1.347	2.724	117.5	125.0
BLYP	6-31G(d,p)	1.487	1.358	2.756	117.8	124.3
BLYP	cc-pVTZ	1.485	1.349	2.730	117.4	125.1
B3PW91	6-31G(d,p)	1.478	1.345	2.720	117.3	125.4
B3PW91	cc-pVTZ	1.474	1.336	2.698	117.3	125.4
B3LYP	6-31G(d,p)	1.480	1.346	2.726	117.6	124.9
B3LYP	cc-pVTZ	1.478	1.338	2.702	117.2	125.6
MPW1PW91	6-31G(d,p)	1.474	1.342	2.715	117.5	125.0
MPW1PW91	cc-pVTZ	1.472	1.334	2.694	117.2	125.5
			2S, UDFT			
SVWN	6-31G(d,p)	1.438	1.355	2.697	117.7	124.7
SVWN	cc-pVTZ	1.437	1.345	2.676	117.5	125.1
BP86	6-31G(d,p)	1.440	1.377	2.710	117.5	125.0
BP86	cc-pVTZ	1.437	1.368	2.692	117.3	125.4
BPW91	6-31G(d,p)	1.436	1.377	2.705	117.4	125.1
BPW91	cc-pVTZ	1.432	1.368	2.686	117.3	125.4
BLYP	6-31G(d,p)	1.446	1.377	2.719	117.5	124.9
BLYP	cc-pVTZ	1.443	1.368	2.701	117.4	125.3
B3PW91	6-31G(d,p)	1.418	1.373	2.676	117.2	125.5
B3PW91	cc-pVTZ	1.414	1.366	2.658	117.1	125.8
B3LYP	6-31G(d,p)	1.422	1.374	2.684	117.3	125.4
B3LYP	cc-pVTZ	1.419	1.366	2.664	117.1	125.8
MPW1PW91	6-31G(d,p)	1.414	1.372	2.670	117.2	125.5
MPW1PW91	cc-pVTZ	1.410	1.365	2.654	117.1	125.8
			2T, UDFT			
SVWN	6-31G(d,p)	1.404	1.373	2.622	116.3	127.3
SVWN	cc-pVTZ	1.398	1.365	2.602	116.2	127.7
BP86	6-31G(d,p)	1.418	1.388	2.656	116.5	127.0
BP86	cc-pVTZ	1.413	1.381	2.638	116.4	127.3
BPW91	6-31G(d,p)	1.417	1.386	2.654	116.5	127.0
BPW91	cc-pVTZ	1.411	1.379	2.636	116.4	127.3
BLYP	6-31G(d,p)	1.421	1.389	2.664	116.6	126.9
BLYP	cc-pVTZ	1.416	1.382	2.646	116.4	127.2
B3PW91	6-31G(d,p)	1.406	1.379	2.640	116.6	126.8
B3PW91	cc-pVTZ	1.401	1.372	2.622	116.4	127.1
B3LYP	6-31G(d,p)	1.409	1.381	2.646	116.6	126.8
B3LYP	cc-pVTZ	1.404	1.373	2.628	116.4	127.1
MPW1PW91	6-31G(d,p)	1.404	1.377	2.637	116.6	126.8
MPW1PW91	cc-pVTZ	1.399	1.370	2.619	116.4	127.1

[a] Distances in Å; bond angles α in degree.

energy of **TS(1−2)**. At RB3LYP−UB3LYP(sum)/6-311+G-(3df,3pd), calculated energy parameters $\Delta_R E$, $\Delta E^{\ddagger}$(**1**−**2**), and $\Delta E^{\ddagger}$(**2**−**1**) are 7.8, 31.8, and 24.0 kcal/mol, respectively, thus deviating from experimental values by just 0, 1.7, and 1.7 kcal/mol, respectively. Hence, RDFT-UDFT/B3LYP(sum)/6-311+G-(3df,3pd) provides the most accurate description of the energetics of the Bergman reaction so far obtained by quantum chemical investigations.

When considering whether BLYP or B3LYP should be applied for the description of the Bergman reaction of enediynes, there are four arguments in favor of the latter functional. (1) Contrary to BLYP, which performs well for VDZ basis sets but poorly for larger basis sets, B3LYP results for the Bergman reaction are improved when the basis set is improved ($\mu = 3.7$, 2.9, 2.7; Table 2). (2) B3LYP results are more consistent than BLYP results as reflected by the σ-parameters of Tables 2 and 3. (3) B3LYP results can substantially be improved with the help of the sum formula, which is not the case for pure density functionals such as BLYP. (4) In general, B3LYP performs better for hydrocarbons and other molecules than BLYP and, therefore, will lead to more reliable results if the electronic systems of the Bergman reaction are compared with other molecules.

While the results obtained in this work suggest that UDFT leads to a reliable description of the Bergman reaction, there is still the contradiction that single determinant KS theory is used to describe a multireference problem such as the biradical **2S**. Hence, the results discussed so far may be just due to fortuitous error cancellation. Since we have investigated in parallel work 14 different enediynes and their cyclization reactions,[33] it is important to clarify whether results obtained for the parent enediyne **1** can also be expected for other enediynes. Therefore, we will address in the next section the question of how UDFT can cope with a multireference problem in general.

4. Use of Unrestricted DFT for a Multireference Problem

In the derivation of the KS formalism, no assumption is made on the character of the system to be described. Thus, even a system with strong static correlation effects and, consequently, distinct multireference character can, in principle, be correctly

described on the basis of a single-determinant spin-restricted KS reference state, with all of the static and dynamic electron correlation effects being covered by the XC-energy functional. (Exceptions are certain low-spin open-shell states, for which the KS reference states consist of several equivalent Slater determinants;[42] such systems are, however, outside the scope of this paper.) However, the situation is different in the case of practical applications of the KS formalism. The available approximations for the XC energy were developed to cover dynamic electron correlation effects utilizing often the homogeneous electron gas as a starting point. Accordingly, the functionals used today perform poorly when electronic systems with static correlation effects have to be described. As a consequence, the spin-restricted solution mostly gives a qualitatively incorrect description of a multireference system and (see section 3) becomes externally unstable; that is, there is a transition from spin-restricted to spin-unrestricted DFT. In the case of singlet biradicals such as **2S**, the energetically lowest state is one with an incorrect spin symmetry. More strictly speaking, there are two such solutions, which are equivalent to each other.

Static Correlation Effects and UDFT. Spin-symmetry breaking at the UDFT level is formally similar to that in HF theory, but the background is somewhat different. In HF theory, the closed-shell state is described by the single-determinant S state with the lowest energy. In the simplest case, the broken-symmetry UHF ground state is a mixture of a two-reference S state (ground state and doubly excited state) and a single-reference T state, the weighted average energy of which may be lower than the energy of the RHF S ground state. In DFT, however, one would get a spin-symmetric KS state if one had the exact functional available, i.e., the spin-restricted solution would be stable for the description of singlet biradicals, on which we focus in this work. In KS calculations with approximate functionals, symmetry breaking in the KS ground state simply reflects the shortcomings of the approximate functionals used. Considering that the KS density (spin density, total density, on-top pair density; see below) corresponds to a many-particle wave function, the broken-symmetry KS state represents a many-particle state that is a mixture of a S and a T state, i.e., a state with spin contamination, in a way similar to that discussed for UHF. (Note that the KS wave functions are associated with the fictitious system of noninteracting electrons, even though it leads in the ideal case to the correct one-electron density.)

The descriptions provided by UDFT and UHF are closely related, only the causes for symmetry breaking are different. In HF theory, it is a failure of the method and in DFT, a failure of the approximate functional used. This has to be considered when analyzing the usefulness of these approaches or trying to cure their failures. While a frequently applied approach in wave function theory is to cure the failure by spin-projection methods,[43] this clearly makes little sense as a correction for a poor functional in the case of DFT and explains the failures encountered in this direction.[44]

In both UHF and UDFT, the use of a broken-symmetry state allows static correlation effects to be described, which are missing in restricted HF and DFT, respectively. In calculations of typical multireference systems, the static correlation effects are formally covered as a part of the exchange energy.[45] Clearly, this situation can be improved when DFT exchange is calibrated with the help of experimental data, as is the case in hybrid functional theory.[40] In so far, it is fair to say that B3LYP and other hybrid methods are semiempirical methods designed to better cover static correlation effects (and, of course, lacking dynamic correlation effects) via the exchange functional. The performance of the hybrid functional depends of course on its semiempirical calibration by experimental reference data where the instability of hybrid functionals can lead nevertheless to unforeseen failures. In summary, however, UDFT and in particular UDFT with hybrid functionals provide a basis for a reasonable description of multireference systems with significant static electron correlation. However, the question is how reliable is such a description. In UHF theory, the answer to this question is based on a quantitative assessment of spin contamination. Therefore, the question of spin contamination has also to be discussed for UDFT.

Spin Contamination in UDFT. In the literature, the spin symmetry of a KS state is often investigated as if the KS Slater determinant were the wave function of the real state, i.e., the spin operator or a spin projection operator is applied to the KS determinant of this state.[34] Wang and co-workers[46] investigated a number of high-spin states of atoms and small molecules (both radicals and T biradicals) and compared the $\langle \hat{S}^2 \rangle$ values computed from the KS Slater determinant with values obtained by an approximate approach based on the correct Löwdin formula[47] for $\langle \hat{S}^2 \rangle$. They found that the values from the KS Slater determinant, though not exact, are at least reasonable for high-spin radicals and biradicals.

Although this investigation may be considered as some justification for using the KS determinant to assess the role of spin contamination in UDFT, a strong caveat is necessary— The cases investigated by Wang and co-workers[46] were exclusively those with small spin contamination where an error in the calculated $\langle \hat{S}^2 \rangle$ does not matter too much. The situation of singlet biradicals or, in general, that of electronic systems with high spin contamination is different and more problematic. The UHF description of a singlet biradical often contains 50% contamination by T, quintet, etc., states where the T contamination is the dominant one. This information is obtained by calculating $\langle \hat{S}^2 \rangle$, and it is used as a motivation for applying spin-projected methods or replacing single-determinant theory by multiconfiguration theory. These improvements are necessary because in wave function theory results are sensitive to any contamination of the wave function used. The consequences of spin contamination in DFT are not exactly known, but there is a strong indication that DFT densities and energies are less affected by spin contamination. In any case, it is not justified to calculate $\langle \hat{S}^2 \rangle$ with the help of the KS determinant and to draw from the results any conclusion as for the correctness of calculated DFT energies. There are three reasons why the use of $\langle \hat{S}^2 \rangle$ as a diagnostic for the quality of UDFT descriptions of S biradicals has to be questioned.

(1) The KS wave function corresponds to the situation of noninteracting electrons, which differs considerably from the many-particle state represented by the KS density. Hence, one cannot expect that $\langle \hat{S}^2 \rangle$ calculated from the KS Slater determinant has any physical significance.

(2) The expectation value $\langle \hat{S}^2 \rangle$ is a two-particle quantity, whereas the KS wave function should only reproduce one-particle quantities, viz., ρ_α and ρ_β, correctly. There is no reason that the KS Slater determinant yields the correct $\langle \hat{S}^2 \rangle$ and an expectation value for $\hat{S}^2$ that deviates from $S(S + 1)$ does not necessarily indicate spin contamination.

(3) At present, the correct calculation of $\langle \hat{S}^2 \rangle$ with the KS density is an unresolved problem.

In view of points 1−3 above, it is understandable that various authors have suggested to ignore $\langle \hat{S}^2 \rangle$ calculated from the KS determinant, even for the case that the KS orbitals cover

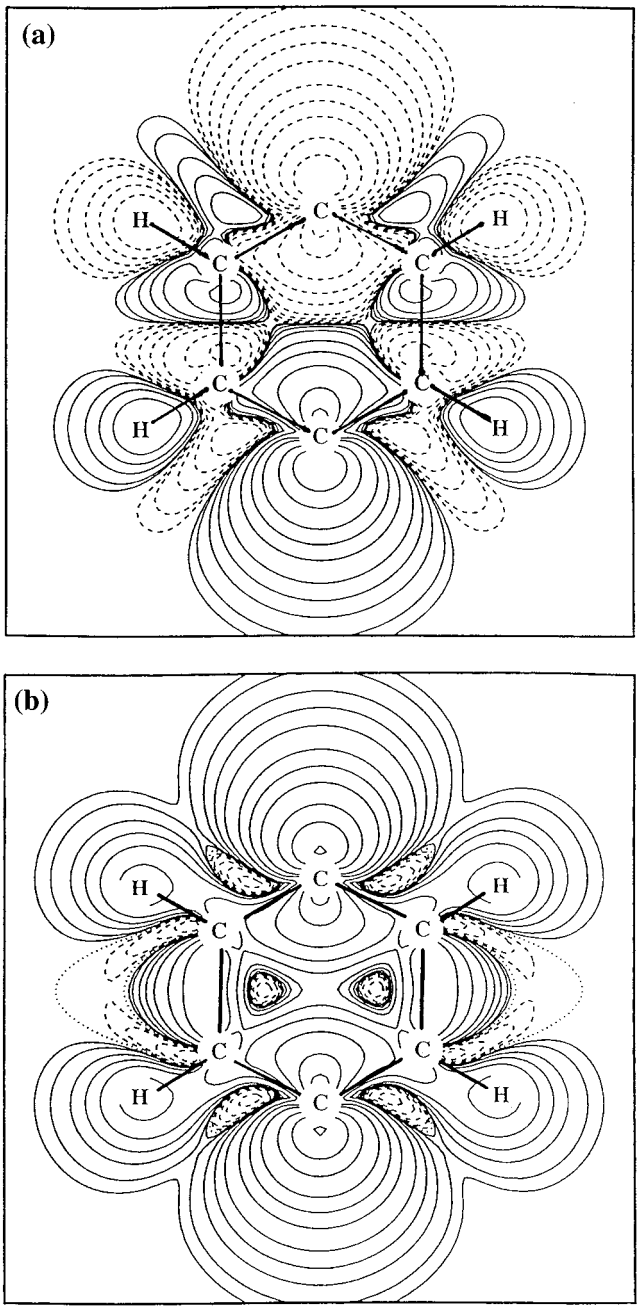

Figure 4. Spin density distribution $m_s(\mathbf{r}) = \rho_\alpha(\mathbf{r}) - \rho_\beta(\mathbf{r})$ given in form of a contour line diagram in the plane of the molecule for (a) the S state and (b) the T state of *p*-didehydrobenzene **2** as calculated at the UB3LYP/cc-pVTZ level of theory. Solid lines indicate a surplus of α spin, dashed lines, a surplus of β spin, and the dotted line the zero level. The geometry has been optimized at the UB3LYP/cc-pVTZ level for **2S** and used for **2T** to make a direct comparison between the S and T state possible. The following contour lines are used: 0, ±0.0001, ±0.0002, ±0.0005, ±0.001, ±0.002, ±0.005, ±0.01, ±0.02, ±0.05, ±0.1, and ±0.2 e/bohr^3.

important properties of the HF orbitals.[48] It is a contradiction in itself to use spin-projection methods developed within wave function theory in the case of UDFT. Pople, Gill, and Handy[49] argue that the spin-unrestricted KS formalism is the appropriate formulation of the KS approach for spin-resolved DFT and that there is no motivation to avoid or remedy an incorrect value of $\langle \hat{S}^2 \rangle$ for the KS Slater determinant by a spin-restricted KS formalism or some kind of spin-projection technique.

Investigation of Spin Densities. Spin contamination and the expectation value $\langle \hat{S}^2 \rangle$ for KS singlet states with broken spin symmetry can be determined with the help of the spin (magnetization) density distribution $m_s(\mathbf{r}) = \rho_\alpha(\mathbf{r}) - \rho_\beta(\mathbf{r})$. A nonvanishing spin density in an S biradical represents definite evidence for spin contamination, because for a noncontaminated state with $N_\alpha = N_\beta$ the spin density should vanish everywhere. In Figure 4a, the spin density $m_s(\mathbf{r})$ for the symmetry-broken S state of **2** calculated at UB3LYP/cc-pVTZ is shown in the form of a contour line diagram, where solid contour lines denote a surplus of α- and dashed contour lines a surplus β-spin density. Clearly, the surplus of α-spin density at C6 (see Figure 1) indicates that the S state is contaminated by a T state with $M = 0$. If one uses the localized orbitals *a* and *b* (see Figure 3) as obtained in a U description to form the wave functions for S and T, the corresponding densities $\rho_s(\mathbf{r})(s = \alpha, \beta)$ can be directly determined. The spin density $m_s(\mathbf{r})$ is given by the expression $a^2 - b^2$ which leads to the $m_s(\mathbf{r})$ shown in Figure 4a. The many-particle state represented by the spin density $m_s(\mathbf{r})$ is a mixture of S and T component, possibly augmented by higher-spin components. This mixing also accounts for the fact that the spin density of the system has a lower symmetry than the molecule itself.

We will investigate whether one can estimate the weight of the T component and, accordingly, $\langle \hat{S}^2 \rangle$ from the spin density of this broken-symmetry state and the spin density of the corresponding T state shown in Figure 4b. This will require three approximations and assumptions. First, we have to assume that the broken-symmetry state represents a mixture of just S and T states, which is insofar justified because the $S + 1$ component normally is the dominant contamination in an U description. Second, we will have to retreat to wave function theory and decompose the broken-symmetry KS Slater determinant into its S and T component, which is not strictly justified. Finally, we will assume that the T component in the broken-symmetry state is equivalent to the T state of the molecule. With these approximations, it is possible to get a value for $\langle \hat{S}^2 \rangle_{m_s}$ based on the UDFT spin densities $m_s(\mathbf{r})$.

The broken-symmetry KS state can be written as

$$|\Phi_{\mathrm{UDFT}}\rangle = \hat{a}_\alpha^\dagger \hat{b}_\beta^\dagger |\mathrm{core}\rangle \tag{3}$$

where *a* and *b* are the orbitals of the two unpaired electrons (Figure 3a) and the core is assumed to be spin-unpolarized. The spin density of the state is

$$m_s^{\mathrm{UDFT}}(\mathbf{r}) = a^2(\mathbf{r}) - b^2(\mathbf{r}) \tag{4}$$

By decomposing $|\Phi_{\mathrm{UDFT}}\rangle$ into S and T components, one finds that

$$\begin{aligned} \langle \hat{S}^2 \rangle_{\mathrm{UDFT}} &= \langle \Phi_{\mathrm{UDFT}} | \hat{S}^2 | \Phi_{\mathrm{UDFT}} \rangle \\ &= 1 - \langle a|b \rangle^2 \end{aligned} \tag{5}$$

For the triplet KS state, it is

$$|\Phi_{\mathrm{UDFT}}\rangle = C \hat{a}_\alpha^\dagger \hat{b}_\alpha^\dagger |\mathrm{core}\rangle \tag{6}$$

$$\begin{aligned} C &= [1 - \langle a|b \rangle^2]^{-1/2} \\ &= \langle \hat{S}^2 \rangle_{\mathrm{UDFT}}^{-1/2} \end{aligned} \tag{7}$$

The spin density for this case becomes

$$m_s^{\mathrm{T}}(\mathbf{r}) = \frac{1}{\langle \hat{S}^2 \rangle_{\mathrm{UDFT}}} [a^2(\mathbf{r}) + b^2(\mathbf{r}) - \sqrt{1 - \langle \hat{S}^2 \rangle_{\mathrm{UDFT}}}\, a(\mathbf{r})\, b(\mathbf{r})] \tag{8}$$

By comparing eqs 4 and 8, one finds that the two spin densities are proportional to each other in regions where one of the two orbitals dominates and that one can determine $\langle \hat{S}^2 \rangle_{\mathrm{UDFT}}$ directly from the proportionality factor

$$|m_s^{\mathrm{UDFT}}(\mathbf{r})| = \langle \hat{S}^2 \rangle_{\mathrm{UDFT}} m_s^{\mathrm{T}}(\mathbf{r}) \quad \text{for} \quad |a(\mathbf{r})| \gg |b(\mathbf{r})| \quad \text{or} \quad |b(\mathbf{r})| \gg |a(\mathbf{r})| \quad (9)$$

Hence, to determine $\langle \hat{S}^2 \rangle_{\mathrm{UDFT}}$, one has to find a region in the molecule where one of the open-shell orbitals with its electron population contributes predominantly to the spin density. Such a region can be found either by knowing the electronic structure of the molecule or with the help of the relative spin polarization $\zeta(\mathbf{r}) = (\rho_\alpha(\mathbf{r}) - \rho_\beta(\mathbf{r}))/\rho(\mathbf{r})$. For this region, one has to fit m_s^{UDFT} to the ansatz $m_s^{\mathrm{UDFT}} = f m_s^{\mathrm{T}}$ according to a least-squares criterion. Utilizing eq 9, factor f leads to a reasonable estimate for $\langle \hat{S}^2 \rangle_{\mathrm{UDFT}}$, in the following denoted as $\langle \hat{S}^2 \rangle_{m_s}$. Then, $\langle \hat{S}^2 \rangle_{m_s}$ can be used in connection with eq 2b to determine the percentage of S character with the help of the factor x.

We used eq 9 to estimate $\langle \hat{S}^2 \rangle_{m_s}$ for UDFT/cc-pVTZ descriptions of biradical **2S** employing the functionals SVWN, BLYP, and B3LYP, which can be considered to be typical representatives for a LSD, GGA, and hybrid functional approach. In view of the discussion given above, the fits were done along the outer bisector of the C5−C6−C1 bond angle. Parts a−c of Figure 5 show the spin density $m_s(\mathbf{r})$ along this line for the broken-symmetry (solid line) and the T state (dashed line) of **2S**. The spin density $m_s(\mathbf{r})$ possesses a shell structure close to the nucleus, which is probably due to differences in the α and β KS core orbitals. Therefore, we restrict the fit procedure to the region 0.5−3 Å from the C6 nucleus. For B3LYP and BLYP, the ratio of the two spin densities $m_s(\mathbf{r})$ is nearly constant in this region; however, it varies for larger distances in the case of the SVWN functional. Still, the least-squares fit gives reliable results in all cases, because the deviations in the SVWN case occur for small absolute values of $m_s(\mathbf{r})$ and thus have little influence on the fit. The results, shown in Table 6, indicate that in the case of **2** (1) spin contamination is underestimated up to 22% when using KS orbitals for the calculation of $\langle \hat{S}^2 \rangle$; (2) errors in $\langle \hat{S}^2 \rangle$ obtained from KS orbitals are largest for SVWN, but smallest for B3LYP; (3) errors in energy corrections, e.g., based on the sum formula (1) may be as high as 37% if one considers the S−T splitting of pure density functionals such as SVWN.

These results confirm that $\langle \hat{S}^2 \rangle$ calculated from UDFT orbitals still has some diagnostic value in the way that a large (small) spin contamination leads also to a large (small) deviation of the $\langle \hat{S}^2 \rangle_{\mathrm{KS}}$ value from the ideal value. Since SVWN leads to a rather stable RDFT description of **2S** (see section 3), the $\langle \hat{S}^2 \rangle$ value at SVWN/cc-pVTZ is relatively small; however, the reliability of the KS orbital description for spin contamination is also small in contrast to the B3LYP result (approximately 1:1 mixing of S and T, small difference between $\langle \hat{S}^2 \rangle$ values; see Table 6). This observation helps to elucidate one of the major deficiencies of the use of the KS determinant for the calculation of $\langle \hat{S}^2 \rangle$. If the UDFT state of the biradical **2S** is close to a 1:1 mixture of S and T, the description of the S wave function in terms of localized orthogonal orbitals a and b is close to the real wave function and well-represented by the KS determinant. As soon as the S state dominates the UDFT state, orbitals a and b will no longer be orthogonal and will start to overlap. This implies that the orbitals of an electron-interacting system (e.g., the corresponding natural orbitals) deviate more from the KS orbitals, which is reflected by an increasing difference between $\langle \hat{S}^2 \rangle$ values obtained from the KS spin density $m_s(\mathbf{r})$ and from KS orbitals. We conclude that in the case of S biradicals, the diagnostic value of $\langle \hat{S}^2 \rangle_{\mathrm{KSorbitals}}$ becomes critical because there is an unequal mixing between S and T in the UDFT state.

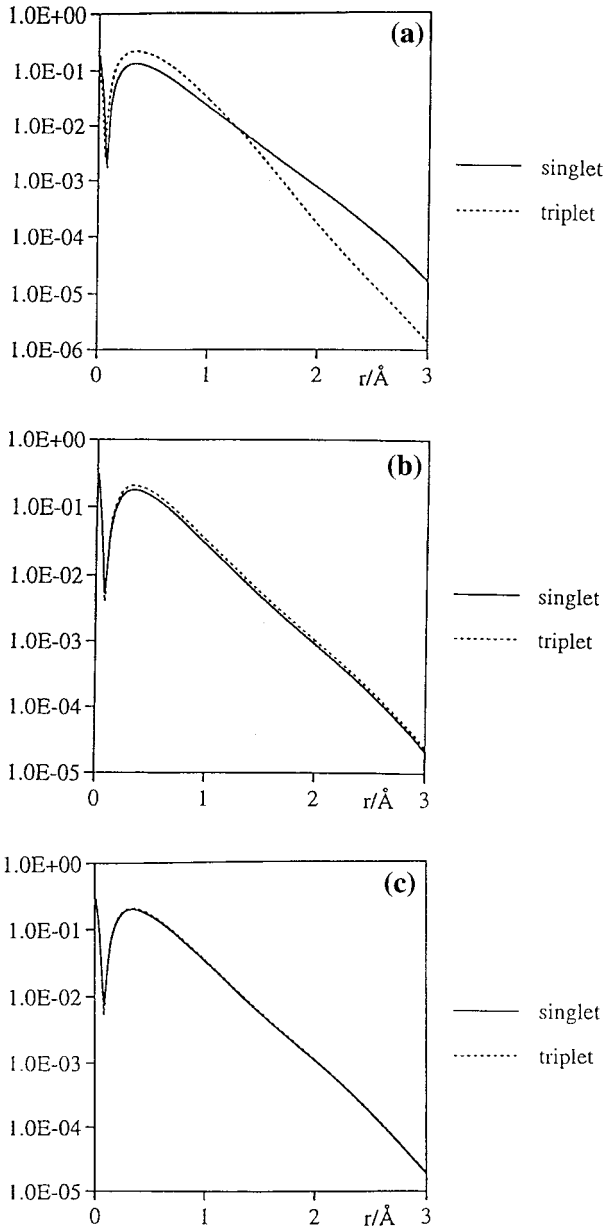

Figure 5. Spin density distribution $m_s(\mathbf{r}) = \rho_\alpha(\mathbf{r}) - \rho_\beta(\mathbf{r})$ for the S state (solid line) and the T state (dashed line) of *p*-didehydrobenzene along the outer bisection of the bond angle C5−C6−C1 as calculated at the (a) USVWN/cc-pVTZ, (b) UBLYP/cc-pVTZ, and (c) UB3LYP/cc-pVTZ level of theory. The position of nucleus C6 defines the zero point of distance r.

Although the spin density $m_s(\mathbf{r})$ can be used to determine the value of $\langle \hat{S}^2 \rangle$, it does not necessarily provide information on the reliability and usefulness of the UDFT energy. In passing, we note that spin magnetization densities (Figure 4) are smaller than 0.01 atomic units on the average, which suggests that spin contamination may be ignored totally for pure density functionals.

The Usefulness of UDFT Results. Perdew, Savin, and Burke (PSB)[35a] developed an alternative interpretation of spin-unrestricted DFT that, while leaving the KS equations unchanged, avoids the symmetry-breaking problems in conventional UDFT. Their approach is based on total and on-top pair

TABLE 6: Description of the UDFT Broken-Symmetry State of 2S with the Help of KS Orbitals and the KS Spin Density $m_s(\mathbf{r})$[a]

functional	% singlet $m_s(\mathbf{r})$	% singlet KS orbitals	$\langle\hat{S}^2\rangle_{KS}$	$\langle\hat{S}^2\rangle_{m_s}$	$\Delta\langle\hat{S}^2\rangle$	$\Delta E(S)$ $m_s(\mathbf{r})$	$\Delta E(S)$ KS orbitals
SVWN	69.1	75.5	0.602	0.491	0.111	2.97	2.15
BLYP	56.8	61.7	0.864	0.767	0.097	3.41	2.78
B3LYP	52.4	53.2	0.954	0.939	0.015	2.41	2.28

[a] The percentage of S character is calculated from the fraction x of eq 2 using either the spin density $m_s(\mathbf{r}) = \rho_\alpha(\mathbf{r}) - \rho_\beta(\mathbf{r})$ or Kohn−Sham (KS) orbitals. $\langle\hat{S}^2\rangle_{KS}$ and $\langle\hat{S}^2\rangle_{m_s}$ denote the expectation value of $\hat{S}^2$ calculated from KS orbitals and the spin density $m_s(\mathbf{r})$, respectively. $\Delta E(S)$ is the energy correction for the S−T splitting calculated with eq 1 using the fraction x of eq 2 (see text).

density rather than spin densities ρ_α and ρ_β. The on-top pair density $P(\mathbf{r},\mathbf{r})$ is given by the probability of finding two electrons at the same position $\mathbf{r}$ (one electron *on top* of another), where $P(\mathbf{r})$ is approximated using KS orbitals:[35b]

$$P(\mathbf{r},\mathbf{r}) = \frac{1}{2}\rho^2(\mathbf{r})\{1 - \zeta^2(\mathbf{r})\} = 2\rho_\alpha(\mathbf{r})\,\rho_\beta(\mathbf{r}) \quad (10)$$

PSB[35a] modified the constrained minimization suggested by Levy[50] to determine the KS energy in the same way as the energy functional given by eq 11:

$$\tilde{F}[\rho_\alpha,\rho_\beta] = \min_{\substack{\rho[\Psi](\mathbf{r}) = \rho_\alpha(\mathbf{r}) + \rho_\beta(\mathbf{r}) \\ P[\Psi](\mathbf{r},\mathbf{r}) = 2\rho_\alpha(\mathbf{r})\rho_\beta(\mathbf{r})}} \langle\Psi|\hat{T} + \hat{V}_{ee}|\Psi\rangle \quad (11)$$

where the tilde is used to indicate the dependence on $\rho(\mathbf{r})$ and $P(\mathbf{r},\mathbf{r})$ rather than $\rho_\alpha(\mathbf{r})$ and $\rho_\beta(\mathbf{r})$. The ground-state energy for a certain potential v, the particle number N, and the total spin S become then[35a]

$$\tilde{E}[v;N,S] = \min_{\substack{\rho_\alpha \to N/2+S \\ \rho_\beta \to N/2-S}} \{\tilde{F}[\rho_\alpha,\rho_\beta] + \int d^3r\, v(\mathbf{r})[\rho_\alpha(\mathbf{r}) + \rho_\beta(\mathbf{r})]\} \quad (12)$$

This approach may not be formally exact in all cases, but there are arguments that it yields ground-state energies close to the real ones and that it is more appropriate for the approximate XC-energy functionals than the conventional formalism.

In conventional spin-DFT, the KS reference state has to reproduce the total density $\rho(\mathbf{r})$ and the relative spin polarization ζ of the real state. PSB[35a] abandon the requirement that the reference and the real state should have the same ζ. Also, they suggest that the spin-symmetry breaking in the KS wave function must be understood as a sign of static correlation effects active in the real state.

There is a relation between $\zeta(\mathbf{r})$, $P(\mathbf{r},\mathbf{r})$, and the amount of static correlation effects covered by an UDFT calculation. Because of the Pauli principle, two electrons at the same position must be of different spin. Spin polarization, however, means that one spin dominates and that there is a reduced probability of finding two electrons with opposite spin at a given position. For a given total density, the on-top pair density will decrease with increasing spin polarization because there are less pairs of opposite-spin electrons that can share the same position. On the other hand, static electron correlation effects, which are long-range effects, also will lead to a strong decrease of $P(\mathbf{r},\mathbf{r})$, even in S states, where there is no spin polarization. The on-top pair density thus contains information on both spin polarization and static electron correlation effects. In other words, a local spin polarization of the KS reference function may be related to either spin polarizations or static correlations in the real system; information on static correlation effects is contained in the unrestricted KS reference state and reflected by the exchange functional (see above).

This line of argument can be directly applied to the UDFT description in the way that both KS orbitals (as discussed above) and the KS spin density $m_s(\mathbf{r})$ are considered as intermediate, physically not relevant quantities and that the UDFT results are exclusively analyzed on the basis of the calculated total density and the on-top density.[35a]

Figure 6 shows the on-top density distribution $P(\mathbf{r},\mathbf{r})$ for the S state of biradical **2S** (Figure 6a) and the difference of the S and T on-top pair densities (Figure 6b) in the form of contour line diagrams as calculated from the KS orbitals with eq 10 at the UB3LYP/cc-pVTZ level of theory. For Figure 6b, solid contour lines indicate that the on-top density is larger in the S state and dashed contour lines larger in the T state. The S state possesses a slightly higher on-top density than the T state in the region where the unpaired electrons are located, which is due to the fact that the two unpaired electrons in this state have opposite spin. Accordingly, there is a small probability for them to be at the same position. On the other hand, there are regions (especially the C−C bond regions) where the T state has a higher on-top pair density than the S state. The coupling mechanism between the single electrons of the S state involves (see section 3, Figure 3) the electrons of the CC bonds in the benzene ring. This coupling pattern becomes visible in the difference on-top density of Figure 6b. Coupling increases the on-top density in the CC bonds involving C3 and C6 via π-type overlap (see Figure 3b). Occupation of the σ^* orbitals decreases the on-top density of the S state in the HCCH bonds of **2** relative to that of the T state. The difference on-top density of Figure 6b also suggests that a coupling by a through-space mechanism plays a little role as predicted in section 3.

The on-top densities give a better account of electron correlation in the two states than the spin density does.

(a) Contrary to the spin densities $m_s(\mathbf{r})$, $\rho_\alpha(\mathbf{r})$, and $\rho_\beta(\mathbf{r})$, the on-top pair densities comply with the symmetry of the molecule in both the S and the T state.

(b) For the S state, the symmetry breaking leads to a 2-fold degenerate KS ground state even though the real ground state is not degenerate. Within the alternative interpretation, these two ground states possess the same total and on-top pair density and, therefore, they are equivalent representations of the same KS ground state.

(c) The on-top pair densities for S and T state are very similar to each other, which is in line with the small energy difference of the two states, whereas the spin densities $m_s(\mathbf{r})$ for the two states differ qualitatively from each other.

This supports the point of view given by PSB[35a] and shows that the concept of the on-top pair density is reasonable for the investigation of systems with strong static correlations.

There are more sophisticated ways to use DFT to describe systems with strong static correlations. A number of authors have recently made attempts to combine concepts from multi-

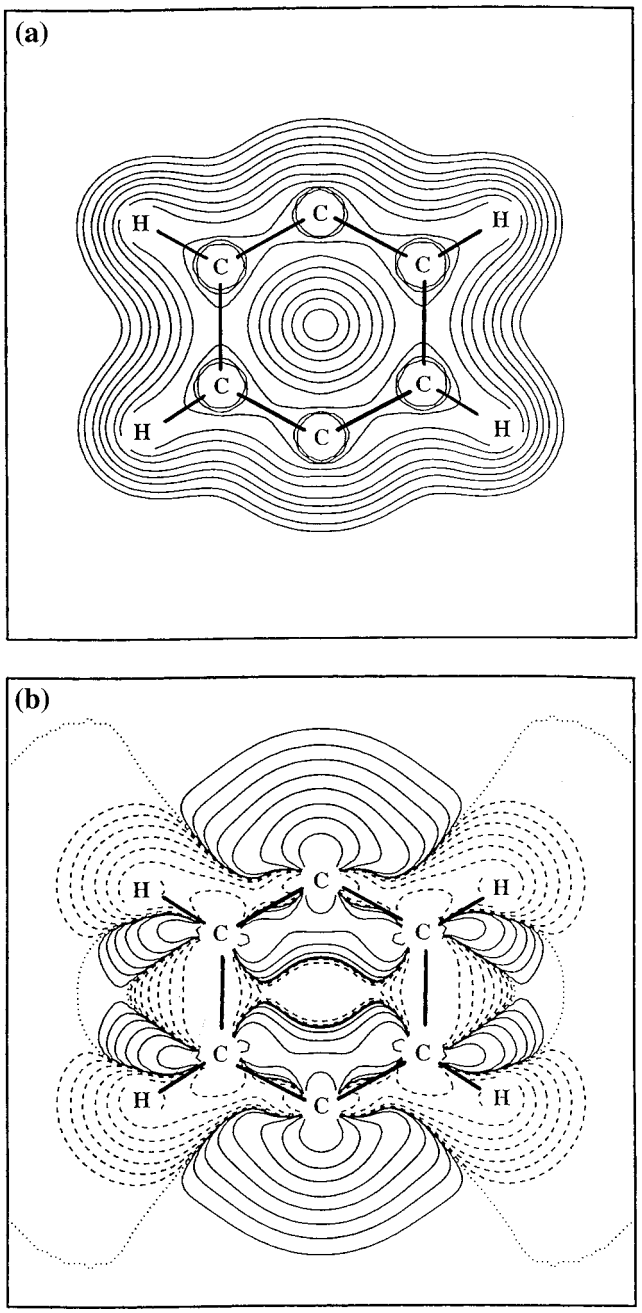

Figure 6. (a) On-top pair density distribution $P(\mathbf{r},\mathbf{r})$ determined with eq 10 given in the form of a contour line diagram in the plane of the molecule for the S state of *p*-didehydrobenzene **2** as calculated at the UB3LYP/cc-pVTZ level of theory. The following contour lines are used: 0.0001, 0.0002, 0.0005, 0.001, 0.002, 0.005, 0.01, 0.02, 0.05, 0.1, and 0.2 au. (b) Difference on-top density distribution $\Delta P(\mathbf{r},\mathbf{r}) = P_{2S}(\mathbf{r},\mathbf{r}) - P_{2T}(\mathbf{r},\mathbf{r})$ given in form of a contour line diagram in the plane of the molecule as calculated at the UB3LYP/cc-pVTZ level of theory. Solid lines indicate a higher value for the S state, dashed lines, a higher value for the *T* state, and the dotted line indicates equal values for both states. The geometry was optimized at the UB3LYP/cc-pVTZ level for **2S** and used for **2T** to make a direct comparison between the S and T state possible. The following contour lines are used: 0, $\pm 3 \times 10^{-7}$, $\pm 10^{-6}$, $\pm 3 \times 10^{-6}$, $\pm 10^{-5}$, $\pm 3 \times 10^{-5}$, $\pm 10^{-4}$, $\pm 3 \times 10^{-4}$, and $\pm 10^{-3}$ e/bohr^3.

reference ab initio theory and DFT to get cheap yet reliable methods to describe such systems.[36,42,51,52] However, these methods are considerably more expensive than UDFT and, therefore, it will be of great value if one can motivate for a given problem as done in this work for the low-spin biradical **2** that UDFT provides a reasonable description of such systems.

5. Conclusions

A basic prerequisite for a correct assessment of the performance of DFT in the case of the Bergman reaction is that experimental results obtained at different temperatures (reaction enthalpy at 298 K; activation enthalpy at 470 K) are referenced to the same standard. Since in this work primarily electronic effects were discussed, energies at 0 K (without ZPE corrections) have been chosen by taking vibrational and temperature corrections from theory to convert enthalpies from experiment to energies at 0 K. We note that this point (as well as the stability question, the performance of UDFT, and the advantages of hybrid functionals) was overlooked in previous DFT investigations of the Bergman reaction, thus leading to this improved performance test of DFT. The following conclusions can be drawn from our analysis.

(1) A basic prerequisite for the correct description of the Bergman reaction of **1** is to monitor the stability of RDFT along the reaction path. **TS(1−2)** is stable at RDFT, although the stability parameter λ is rather small. For biradical **2S**, all functionals and basis sets used in this work lead to an unstable RDFT description.

(2) The instability of DFT functionals increases from LSD to GGA and hybrid methods, which is a direct consequence of the way in which exchange and dynamic electron correlation effects are covered by these functionals. A LSD functional, for which electron exchange and electron correlation are derived from the homogeneous electron gas, should always be more stable than a hybrid functional, which possesses HF exchange. By using larger basis sets, one can slightly improve the stability of a given functional, which can be interpreted in the way that more correlation effects are covered.

(3) The RDFT description of biradical **2** leads to wrong S−T splittings, an unrealistic geometry, and a falsification of the DFT energetics of the Bergman reaction. This is a direct result of the necessity of exaggerating through-bond interactions to couple the single electrons of **2** at the RDFT level. This was overlooked in previous DFT investigations.[12,13]

(4) UDFT considerably improves the description of biradical **2** because of the fact that static electron correlation effects are covered at this level. It is argued that this is a result of the different description of exchange correlation effects when replacing RDFT by UDFT.

(5) LSD and GGA functionals underestimate the barrier of the Bergman reaction of **1**, which has also been found in other cases and which was not observed previously because comparison with experimental data at different temperatures was carried out indiscriminately.

(6) A reliable description of the Bergman reaction of **1** is obtained at the RDFT-UDFT/B3LYP level of theory. Despite the instability of the hybrid functional, its semiempirical calibration, which may also cover lacking static correlation effects, leads to a better description of the barrier. Highest accuracy is obtained with the TZP basis sets. At RB3LYP-UB3LYP/6-311+G(3df,3pd), calculated values of $\Delta_R E$, $\Delta^{\ddagger}E$(**1**−**2**, and $\Delta^{\ddagger}E$(**2**−**1**) are 10.1, 34.1, and 24.0 kcal/mol, respectively, corresponding to $\Delta\Delta_R H_0^f(298) = 10.8$, $\Delta^{\ddagger}H$(**1**−**2**,470) = 32.2 and $\Delta^{\ddagger}H$(**2**−**1**,470) = 22.1 kcal/mol in reasonable agreement (mean absolute deviation of 2.7 kcal/mol) with experimental values of 8.5 ± 1.0, 28.23 ± 0.5, and 19.75 ± 0.7 kcal/mol, respectively (see Figure 1 and ref 5).

(7) We suggest for B3LYP and other hybrid functionals use of the sum formula (1) thus yielding at RB3LYP-UB3LYP-(sum)/6-311+G(3df,3pd) $\Delta\Delta_R H_0^f(298) = 8.5$, $\Delta^{\ddagger}H$(**1**−**2**,470) = 29.9, and $\Delta^{\ddagger}H$(**2**−**1**,470) = 21.4 kcal/mol, respectively. These

values differ on the average by just 1.1 kcal/mol from experimental results.[5] For the S−T splitting, ΔE(**2S**−**2T**,0), ΔE(**2S**−**2T**,0,sum), ΔH(**2S**−**2T**,298), and ΔH(**2S**−**2T**,298,sum) are 2.6, 4.9, 2.9, and 5.2 kcal/mol, respectively, which are all close to the measured value of 3.5 kcal/mol.[11]

Hence, the RDFT-UDFT(sum)/B3LYP/6-311+G(3df,3pd) description of the Bergman reaction is more accurate than the best previous CCSD(T) result.[10] Clearly, this is due to the correct use of U rather than R theory for the description of biradical **2S**. Analysis of the UDFT description of biradical **2S** leads to the following results.

(8) Symmetry-breaking at the UDFT level results from the necessity of including static correlation effects, which can be covered (a) via the (from RDFT) differing UDFT exchange part and (b) via the semiempirical calibration of hybrid functionals.[35]

(9) The expectation value $\langle\hat{S}^2\rangle$ calculated from KS orbitals differs from that calculated from the spin (magnetization) density distribution $m_s(\mathbf{r})$. A new way of calculating $\langle\hat{S}^2\rangle$ is discussed and differences in calculated $\langle\hat{S}^2\rangle$ values are rationalized.

(10) Following PSB,[35a] we suggest that the quality of the UDFT description is evaluated with the help of total and on-top pair density distribution rather than KS orbitals or the spin density distribution $m_s(\mathbf{r})$ because the former do not suffer from the symmetry-breaking problem. The correct behavior of the on-top pair density guarantees that the UDFT solution leads to a reasonable description of the singlet biradical **2** and, by this, also of the energetics of the Bergman reaction. This was confirmed in parallel investigations on enediynes with heteroatoms.[33]

Acknowledgment. This work was supported by the Swedish Natural Science Research Council (NFR). All calculations were done on the CRAY C90 of the Nationellt Superdatorcentrum (NSC), Linköping, Sweden. The authors thank the NSC for a generous allotment of computer time.

References and Notes

(1) (a) Lee, M. D.; Dunne, T. S.; Siegel, M. M.; Chang, C. C.; Morton, G. O.; Borders, D. B. *J. Am. Chem. Soc.* **1987**, *109*, 3464. (b) Lee, M. D.; Dunne, T. S.; Chang, C. C.; Ellestad, G. A.; Siegel, M. M.; Morton, G. O.; McGahren, W. J.; Borders, D. B. *J. Am. Chem. Soc.* **1987**, *109*, 3466. (c) Golik, J.; Clardy, J.; Dubay, G.; Groenewold, G.; Kawaguchi, H.; Konishi, M.; Krishnan, B.; Ohkuma, H.; Saitoh, K.; Doyle, T. W. *J. Am. Chem. Soc.* **1987**, *109*, 3461. (d) Golik, J.; Clardy, J.; Dubay, G.; Groenewold, G.; Kawaguchi, H.; Konishi, M.; Krishnan, B.; Ohkuma, H.; Saitoh, K.; Doyle, T. W. *J. Am. Chem. Soc.* **1987**, *109*, 3462.

(2) For review articles, see: (a) Lee. M. D.; Ellestad, G. A.; Borders, D. B. *Acc. Chem. Res.* **1991**, *24*, 235. (b) Nicolaou, K. C.; Dai, W.-M *Angew. Chem., Int. Ed. Engl.* **1991**, *30*, 1387. (c) Nicolaou, K. C.; Smith, A. L. *Acc. Chem. Res.* **1992**, *25*, 497. (d) Nicolaou, K. C. *Chem. Br.* **1994**, *30*, 33. (e) Ellestad, G. A.; Zein, N.; Ding, W.-D. *Adv. DNA Sequence Specific Agents* **1992**, *1*, 293. (f) Lee, M. D.; Durr, F. E.; Hinman, L. M.; Hamann, P. R.; Ellestad, G. A. *Adv. Med. Chem.* **1993**, 231.

(3) Borders, D. B.; Doyle, T. W., Eds. *Enediyne Antibiotics as Antitumor Agents*; Marcel Dekker: New York, 1995.

(4) (a) Jones, R. R.; Bergman, R. G. *J. Am. Chem. Soc.* **1972**, *94*, 660. (b) Bergman, R. G. *Acc. Chem. Res.* **1973**, *6*, 25. (c) Lockhart, T. P.; Comita, P. B.; Bergman, R. G. *J. Am. Chem. Soc.* **1981**, *103*, 4082. (d) Lockhart, T. P.; Bergman, R. G. *J. Am. Chem. Soc.* **1981**, *103*, 4091. (e) Gleiter, R.; Kratz, D. *Angew. Chem., Int. Ed. Engl.* **1993**, *32*, 842. (f) Turro, N. J.; Evenzahav, A.; Nicolaou, K. C. *Tetrahedron Lett.* **1994**, *35*, 8089. (g) Kuwatani, Y.; Ueda, I. *Angew. Chem., Int. Ed. Engl.* **1995**, *34*, 1892.

(5) Roth, W. R.; Hopf, H.; Horn, C. *Chem. Ber.* **1994**, *127*, 1765.

(6) Marquardt, R.; Balster, A.; Sander, W.; Kraka, E.; Cremer, D.; Radziszewiski, J. G. *Angew. Chem.* **1998**, *110*, 1001.

(7) (a) Nicolaou, K. C.; Zuccarello, G.; Ogawa, Y.; Schweiger, E. J.; Kumazawa, T. *J. Am. Chem. Soc.* **1988**, *110*, 4866. (b) Snyder, J. P. *J. Am. Chem. Soc.* **1989**, *111*, 7630. (c) Snyder, J. P.; Tipsword, G. E. *J. Am. Chem. Soc.* **1990**, *112*, 4040. (d) Snyder, J. P. *J. Am. Chem. Soc.* **1990**, *112*, 5367. For a differing view, see: (e) Magnus, P.; Carter, P.; Elliott, J.; Lewis, R.; Harling, J.; Pitterna, T.; Bauta, W. E.; Fortt, S. *J. Am. Chem. Soc.* **1992**, *114*, 2544. (f) Magnus, P.; Eisenbeis, S. A. *J. Am. Chem. Soc.* **1993**, *115*, 12627.

(8) (a) Hoffner, J. H.; Schottelius, M. J.; Feichtinger, D.; Chen, P. *J. Am. Chem. Soc.* **1998**, *120*, 376. (b) Cramer, C. J. *J. Am. Chem. Soc.* **1998**, *120*, 6261.

(9) (a) Koga, N.; Morokuma, K. *J. Am. Chem. Soc.* **1991**, *113*, 1907. (b) Wenthold, P. G.; Paulino, J. A.; Squires, R. R. *J. Am. Chem. Soc.* **1991**, *113*, 7414. (c) Wenthold, P. G.; Squires, R. R. *J. Am. Chem. Soc.* **1994**, *116*, 6401. (d) Wierschke, S. G.; Nash, J. J.; Squires, R. R. *J. Am. Chem. Soc.* **1993**, *115*, 11958. (e) Lindh, R.; Persson, B. J. *J. Am. Chem. Soc.* **1994**, *116*, 4963. (f) Lindh, R.; Lee, T. J.; Berhardsson, A.; Persson, B. J.; Karlström, G. *J. Am. Chem. Soc.* **1995**, *117*, 7186. (g) Cramer, C. J.; Nash, J. J.; Squires, R. R. *Chem. Phys. Lett.* **1997**, *277*, 311. (h) Cramer, C. J.; Debbert, S. *Chem. Phys. Lett.* **1998**, *287*, 320.

(10) Kraka, E.; Cremer, D. *J. Am. Chem. Soc.* **1994**, *116*, 4929.

(11) Wenthold, P. G.; Squires, R. R.; Lineberger, W. C. *J. Am. Chem. Soc.* **1998**, *120*, 5279.

(12) Schreiner, P. R. *J. Am. Chem. Soc.* **1998**, *120*, 4184.

(13) Chen, W.-C.; Chang, N.-Y.; Yu, C.-H. *J. Phys. Chem. A* **1998**, *102*, 2484.

(14) (a) Hohenberg, P.; Kohn, W. *Phys. Rev* **1994**, *136*, B864. (b) Kohn, W.; Sham, L. *J. Phys. Rev.* **1965**, *140*, A1133.

(15) For reviews on DFT methods, see for example: (a) Parr, R. G.; Yang, W. *International Series of Monographs on Chemistry 16: Density-Functional Theory of Atoms and Molecules*; Oxford University Press: New York, 1989. (b) *Density Functional Methods in Chemistry*; Labanowski, J. K., Andzelm, J. W., Eds.; Springer: Heidelberg, 1990. (c) *Theoretical and Computational Chemistry, Vol. 2, Modern Density Functional Theory−A Tool For Chemistry*; Seminario, J. M., Politzer, P., Eds.; Elsevier: Amsterdam, 1995. (d) *Chemical Applications of Density Functional Theory*; ACS Symposium Series 629; Laird, B. B., Ross, R. B., Ziegler, T., Eds.; American Chemical Society: Washington, DC, 1996. (e) *Lecture Notes in Physics, Density Functionals: Theory and Applications*; Joubert, D., Ed.; Springer: Heidelberg, 1997. (f) *Recent Advances in Computational Chemistry, Vol. 1, Recent Advances in Density Functional Methods, Part II*; Chong, D. P., Ed.; World Scientific: Singapore, 1997. (g) *Electronic Density Functional Theory, Recent Progress and New Directions*; Dobson, J. F., Vignale, G., Das, M. P., Eds.; Plenum Press: New York, 1998. (h) Gill, P. In *Encyclopedia of Computational Chemistry*; Schleyer, P. v. R., Allinger, N. L., Clark, T., Gasteiger, J., Kollman, P. A., Schaefer, H. F., III, Schreiner, P. R., Eds.; Wiley: Chichester, UK, 1998; Vol. 1, p 678.

(16) Slater, J. C. *Quantum Theory of Molecular and Solids, Vol. 4: The Self-Consistent Field for Molecular and Solids*; Mc-Graw Hill: New York, 1974.

(17) Vosko, S. H.; Wilk, L.; Nusair, M. *Can. J. Phys.* **1980**, *58*, 1200.

(18) Becke, A. D. *Phys. Rev.* **1988**, *A38*, 3098.

(19) Perdew, J. P. *Phys. Rev.* **1986**, *B33*, 8822.

(20) (a) Burke, K.; Perdew, J. P.; Wang, Y. In *Electronic Density Functional Theory: Recent Progress and New Directions*; Dobson, J. F., Vignale, G., Das, M. P., Eds.; Plenum: New York, 1998. (b) Perdew, J. P. In *Electronic Structure of Solids '91*; Ziesche, P., Eschrig, H., Eds.; Akademie Verlag: Berlin, 1991; p 11. (c) Perdew, J. P.; Chevary, J. A.; Vosko, S. H.; Jackson, K. A.; Pederson, M. R.; Singh, D. J.; Fiolhais, C. *Phys. Rev.* **1992**, *B46*, 6671. (d) Perdew, J. P.; Chevary, J. A.; Vosko, S. H.; Jackson, K. A.; Pederson, M. R.; Singh, D. J.; Fiolhais, C. *Phys. Rev.* **1993**, *B48*, 4978. (e) Perdew, J. P.; Burke, K.; Wang, Y. *Phys. Rev.* **1996**, *B54*, 16533.

(21) Lee, C.; Yang. W.; Parr. R. G. *Phys. Rev.* **1988**, *B37*, 785.

(22) See, for example: (a) Perdew, J. P.; Ernzerhof, M.; Zupan, A.; Burke, K. *J. Chem. Phys.* **1998**, *108*, 1522. (b) Wilson, L. C.; Levy, M. *Phys. Rev. B* **1990**, *41*, 12930.

(23) Colle, R.; Salvetti, O. *Theor. Chim. Acta* **1975**, *37*, 329.

(24) (a) Becke, A. D. *J. Chem. Phys.* **1993**, *98*, 5648. See also: (b) Stevens, P. J.; Devlin, F. J.; Chablowski, C. F.; Frisch, M. J. *J. Phys. Chem.* **1994**, *98*, 11623.

(25) Adamo, C.; Barone, V. *Chem. Phys. Lett.* **1997**, *274*, 242.

(26) Becke, A. D. *J. Chem. Phys.* **1996**, *104*, 1040.

(27) Hariharan, P. C.; Pople, J. A. *Theor. Chim. Acta* **1973**, *28*, 213.

(28) Woon, D. E.; Dunning, T. H., Jr. *J. Chem. Phys.* **1993**, *98*, 1358.

(29) Kendall, R. A.; Dunning, T. H., Jr.; Harrison, R. J. *J. Chem. Phys.* **1992**, *96*, 6796.

(30) Krishnan, R.; Frisch, M.; Pople, J. A. *Chem. Phys.* **1980**, *72*, 4244.

(31) Bauernschmitt, R.; Ahlrichs, R. *J. Chem. Phys.* **1996**, *104*, 9047.

(32) Seeger, R.; Pople J. A. *J. Chem. Phys.* **1977**, *66*, 3045.

(33) (a) Kraka. E.; Cremer. D. *J. Am. Chem. Soc.*, submitted. (b) Kraka. E.; Cremer. D. *THEOCHEM*, in press. (c) Kraka. E.; Cremer. D. *J. Comput. Chem.*, in press.

(34) See, for example: (a) Lim, M. H.; Worthington, S. E.; Dulles, F. J.; Cramer, C. J. In *Chemical Applications of Density Functional Theory*; Laird, B. B., Ross, R. B., Ziegler, T., Eds.; ACS Symposium Series 629; American Chemical Society: Washington, DC, 1996; p 402. (b) Ziegler, T.; Rauk, A.; Baerends, E. J. *Theor. Chim. Acta* **1977**, *43*, 261.

(35) (a) Perdew, J. P.; Savin, A.; Burke, K. *Phys. Rev. A* **1995**, *51*, 4531. For a more complete description of $P(\mathbf{r},\mathbf{r})$, see: (b) Burke, K.; Perdew, J. P.; Ernzerhof, M. *J. Chem. Phys.* **1998**, *109*, 3760. (c) Perdew, J. P.; Ernzerhof, M.; Burke, K.; Savin, A. *Int. J. Quantum Chem.* **1997**, *61*, 197.

(36) Miehlich, B.; Stoll, H.; Savin, A. *Mol. Phys.* **1997**, *91*, 527.

(37) Kraka. E.; Gräfenstein, J.; Gauss, J.; Reichel, F.; Olsson, L.; Konkoli, Z.; He. Z.; Cremer, D. *COLOGNE 99*; Göteborg University: Göteborg, Sweden, 1999.

(38) Frisch, M. J.; Trucks, G. W.; Schlegel, H. B.; Scuseria, G. E.; Robb, M. A.; Cheeseman, J. R.; Zakrzewski, V. G.; Montgomery, J. A., Jr.; Stratmann, R. E.; Burant, J. C.; Dapprich, S.; Millam, J. M.; Daniels, A. D.; Kudin, K. N.; Strain, M. C.; Farkas, O.; Tomasi, J.; Barone, V.; Cossi, M.; Cammi, R.; Mennucci, B.; Pomelli, C.; Adamo, C.; Clifford, S.; Ochterski, J.; Petersson, G. A.; Ayala, P. Y.; Cui, Q.; Morokuma, K.; Malick, D. K.; Rabuck, A. D.; Raghavachari, K.; Foresman, J. B.; Cioslowski, J.; Ortiz, J. V.; Stefanov, B. B.; Liu, G.; Liashenko, A.; Piskorz, P.; Komaromi, I.; Gomperts, R.; Martin, R. L.; Fox, D. J.; Keith, T.; Al-Laham, M. A.; Peng, C. Y.; Nanayakkara, A.; Gonzalez, C.; Challacombe, M.; Gill, P. M. W.; Johnson, B.; Chen, W.; Wong, M. W.; Andres, J. L.; Gonzalez, C.; Head-Gordon, M.; Replogle, E. S.; Pople, J. A. *Gaussian 98*, revision A.5; Gaussian, Inc.: Pittsburgh, PA, 1998.

(39) Hoffmann, R.; Imamura, A.; Hehre, W. J. *J. Am. Chem. Soc.* **1968**, *90*, 1499.

(40) (a) Perdew, J. P.; Ernzerhof, M.; Burke, K. *J. Chem. Phys.* **1996**, *105*, 9982. (b) Ernzerhof, M. *Chem. Phys. Lett.* **1996**, *263*, 499. (c) Burke, K.; Ernzerhof, M.; Perdew, J. P. *Chem. Phys. Lett.* **1997**, *265*, 115. (d) Ernzerhof, M.; Perdew, J. P.; Burke, K. *Int. J. Quantum Chem.* **1997**, *64*, 285.

(41) Baker, J.; Muir, M.; Andzelm, J.; Schreiner, A. In *Chemical Applications of Density Functional Theory*; Laird, B. B., Ross, R. B., Ziegler, T., Eds.; ACS Symposium Series 629; American Chemical Society: Washington, DC, 1996; p 342.

(42) (a) Gräfenstein, J.; Kraka, E.; Cremer, D. *Chem. Phys. Lett.* **1998**, *288*, 593. See also: (b) Sander, W.; Wandel, H.; Bucher, G.; Gräfenstein, J.; Kraka, E.; Cremer, D. *J. Am. Chem. Soc.* **1998**, *120*, 8480.

(43) (a) Schlegel, H. B. *J. Chem. Phys.* **1986**, *84*, 4530. (b) Schlegel, H. B. *J. Phys. Chem.* **1988**, *92*, 3075. (c) Knowles, P. J.; Handy, N. C. *J. Phys. Chem.* **1988**, *92*, 3097. (d) Chen, W.; Schlegel, H. B. *J. Chem. Phys.* **1994**, *101*, 5957.

(44) Wittbrodt, J. M.; Schlegel, H. B. *J. Chem. Phys.* **1996**, *105*, 6574.

(45) While for UDFT the static correlation energy is contained explicitly in the DFT exchange energy in the HF case, static electron correlation effects are covered implicitly by Coulomb self-interactions, which are larger in the unrestricted than the restricted case. Considering a diatomic molecule (the situation is similar for the biradicals considered in this work), the UHF spin−orbitals are more localized than the RHF space orbitals. Consequently, self-interactions are smaller in the RHF description. Assuming that RHF and UHF description lead to the same Coulomb repulsion energy, deduction of the exchange energy (which contains the self-interaction energy) leads to smaller (more negative) electron interaction energy and total energy in the unrestricted case. This decrease in the UHF energy can be considered to mimic static correlation effects.

(46) Wang, J.; Becke, A. D.; Smith, V. *J. Chem. Phys.* **1995**, *102*, 3477.

(47) Löwdin, P. O. *Phys. Rev.* **1955**, *97*, 1474; (b) **1955**, *97*, 1490.

(48) For a discussion of KS orbitals, see: Stowasser, R.; Hoffmann, R. *J. Am. Chem. Soc.* **1999**, *121*, 3414.

(49) Pople, J.; Gill, P. M. W.; Handy, N. C. *Int. J. Quantum Chem.* **1995**, *56*, 303.

(50) Levy, M. *Proc. Natl. Acad. Sci. U.S.A.* **1979**, *76*, 6062.

(51) (a) Borowski, P.; Jordan, K. D.; Nichols, J.; Nachtigall, P. *Theor. Chem. Acta* **1998**, *99*, 35. (b) Filatov, M.; Shaik, S. *J. Chem. Phys.* **1999**, *110*, 116.

(52) Gräfenstein, J.; Cremer, D. *Chem. Phys. Lett.* **2000**, *316*, 569.